Article

Aromatic stacking facilitated self-assembly of ultra-short ionic complementary peptide sequence: #-sheet nanofibres with remarkable gelation and interfacial properties

Jacek K. Wychowaniec, Ronak Patel, James Leach, Rachel Mathomes, Vikesh Chhabria, Yogita Patil-Sen, Araida Hidalgo-Bastida, Robert T. Forbes, Joseph M. Hayes, and Mohamed A. Elsawy

Biomacromolecules, **Just Accepted Manuscript** • DOI: 10.1021/acs.biomac.0c00366 • Publication Date (Web): 13 May 2020

Just Accepted

is published by the American Chemical Society. 1155 Sixteenth Street N.W., Washington, DC 20036

Aromatic stacking facilitated self-assembly of ultra-short ionic complementary peptide sequence: β-sheet nanofibres with remarkable gelation and interfacial properties

Jacek K. Wychowaniec,[a,b,c] Ronak Patel,[d] James Leach,[d] Rachel Mathomes,[d] Vikesh Chhabria,[d] Yogita Patil-Sen,[d] Araida Hidalgo-Bastida,[e,f,g] Robert T. Forbes,[d] Joseph M. Hayes,[d] Mohamed A. Elsawy*[a,b,d,h]

[a] School of Materials, University of Manchester, Oxford Road, Manchester M13 9PL, UK
[b] Manchester Institute of Biotechnology, Oxford Road, Manchester M13 9PL, UK
[c] School of Chemistry, University College Dublin, Belfield, Dublin 4, Ireland
[d] School of Pharmacy and Biomedical Sciences, University of Central Lancashire, Preston PR1 2HE, UK
[e] Centre for Biosciences, Department of Life Science, Manchester Metropolitan University, Manchester, M1 5GD, UK
[f] Centre for Musculoskeletal Science and Sports Medicine, Manchester Metropolitan University, Manchester, M1 5GD, UK
[g] Centre for Advance Materials and Surface Engineering, Manchester Metropolitan University, Manchester, M1 5GD, UK
[h] Leicester Institute of Pharmaceutical Innovation, Leicester School of Pharmacy, De Monfort University, The Gateway, Leicester LE1 9BH, UK

* Corresponding author: Phone: +44(0)1163664581; e-mail: mohamed.elsawy@dmu.ac.uk

Abstract

Understanding peptide self-assembly mechanisms and stability of the formed assemblies is crucial for development of functional nanomaterials. Herein, we have adopted rational design approach to demonstrate how minimal structural modification to a non-assembling ultra-short ionic self-complementary tetrapeptide *F*E*F*K (Phe4) remarkably enhanced stability of self-assembly into β-sheet nanofibres and induced hydrogelation. This was achieved by replacing flexible phenylalanine residue (*F*) by the rigid phenylglycine (*Phg*) resulting in constrained analogue *Phg*E*Phg*K (Phg4), which positioned aromatic rings in an orientation favourable for aromatic stacking. Phg4 self-assembly into stable β-sheet ladders was facilitated by π-staking of aromatic sidechains alongside hydrogen bonding between backbone amides along the nanofibre axis. The contribution of these non-covalent interactions in stabilising self-assembly was predicted by *in silico* modelling using molecular dynamics simulations and semi-empirical quantum mechanics calculations. In aqueous medium, Phg4 β-sheet nanofibres entangled at a critical gelation concentration $\geq$ 20 mg/mL forming a network of nanofibrous hydrogel. Phg4 also demonstrated unique surface activity in presence of immiscible oils and was superior to commercial emulsifiers in stabilising oil-in-water emulsions. This was attributed to interfacial adsorption of amphiphilic nanofibrilles forming nanofibrillised microspheres. To our knowledge, Phg4 is the shortest ionic self-complementary peptide rationally designed to self-assemble into stable β-sheet nanofibres capable of gelation and emulsification. Our results suggest that Ultra-short Ionic-complementary Constrained Peptides or UICPs have significant potential for the development of cost-effective, sustainable and multifunctional soft bionanomaterials.

Keywords

Peptides, self-assembly, β-sheet, phenylglycine, hydrogels, emulsions

Introduction

Molecular self-assembly has been exploited in nature for the engineering of complex higher macromolecular structures of the proteome. Inspired by nature, the bottom-up design of *de novo* self-assembling peptides has been extensively investigated in the last three decades to innovate a wide variety of stable nanostructures for biomedical applications.[1,2] Zhang and co-workers were the first to propose the self-assembling ionic self-complementary peptide sequence pattern, with alternation of hydrophobic (A) and hydrophilic charged (B) amino acids: $(ABAB)_n$, where n is the number of the pattern repeats.[3,4] This design was inspired by the unusual sequence pattern EAK16 identified in a segment of the Z-DNA binding protein Zuotin, which was purified from the nuclear extract of the baker's yeast *Saccharomyces cerevisiae*.[5]

Peptides based on this sequence pattern were shown to self-assemble into stable β-sheet nanofibres, with typically ~8-16 residues (n=2-4) required to maintain the thermodynamic stability of the assembled nanostructures.[3,4,6-12] Interestingly, the tetrapeptide *F*E*F*K (Phe4), which is the shortest reported sequence with the ABAB pattern (n=1), failed to self-assemble into stable β-sheet structures, implicating the importance of the sequence length for the stability of the formed assemblies (Figure 1A).[8,9] This could possibly be attributed to the fact that longer sequences provide more backbone amide bonds readily available for inter-molecular H-bonding between peptide chains, stabilising the assembled β-sheet structures.

Herein, we investigated whether the structural modification of Phe4 to the more constrained phenylglycine based analogue Phg4 (Figure 1B) would lead to self-assembly into stable amphiphilic β-sheet fibres in aqueous medium and formation of a hydrogel. Our hypothesis was that the introduction of the rigid phenylglycine (*Phg*) residue would result in a more constrained sequence with the aromatic rings directly attached to the peptide backbone readily positioned for inter-molecular π-staking (Figure 1B). This will help stabilise the assembled peptide chains alongside H-bonds formation between the chains backbone amides along the fibre axis, forming a stable amphiphilic β-sheet ladder (Figure 1C).[14,15] A single ladder will in turn interact with a second one through lateral π-interactions of the aromatic rings, which become packed between the dimer ladders shielding the hydrophobic faces from the surrounding aqueous medium (Figure 1C). Further lateral growth of the packed fibres can happen through the possible electrostatic interaction between the exposed charged E and K residues sidechains, forming thicker fibre bundles (Figure 1C). To rationalise the observed effectiveness of Phg4 self-assembly at the atomic level and confirm the role of the aforementioned non-covalent interactions in stabilising self-assembly, we have performed *in silico* modelling on the packed dimer ladder in the form of Prime minimisation and sidechain predictions, molecular dynamics (MD) simulations and semi-empirical quantum mechanics (SQM) calculations.

We have also investigated the interfacial activity of the unpacked amphiphilic β-sheet ladder, which is in thermodynamic equilibrium with the packed form, for stabilising oil-in-water emulgels in biphasic media (Figure 1C).[16-19] Emulgels stability was tested versus a number of commercial emulsifiers under a range of environmental and storage conditions. For these investigations a variety of techniques were used for the molecular, mesoscopic, macroscopic and mechanical characterisation of both hydrogels and emulgels; mainly including Fourier transform infrared spectroscopy (FTIR), scanning electron microscopy (SEM), transmission

electron microscopy (TEM), atomic force microscopy (AFM), small angle x-ray scattering (SAXS), and oscillatory shear rheology.

We have demonstrated the importance of understanding the mechanisms of peptide self-assembly and stability of the assembled structures at a molecular level, which are of paramount importance for the rational engineering of peptide based nanomaterials.

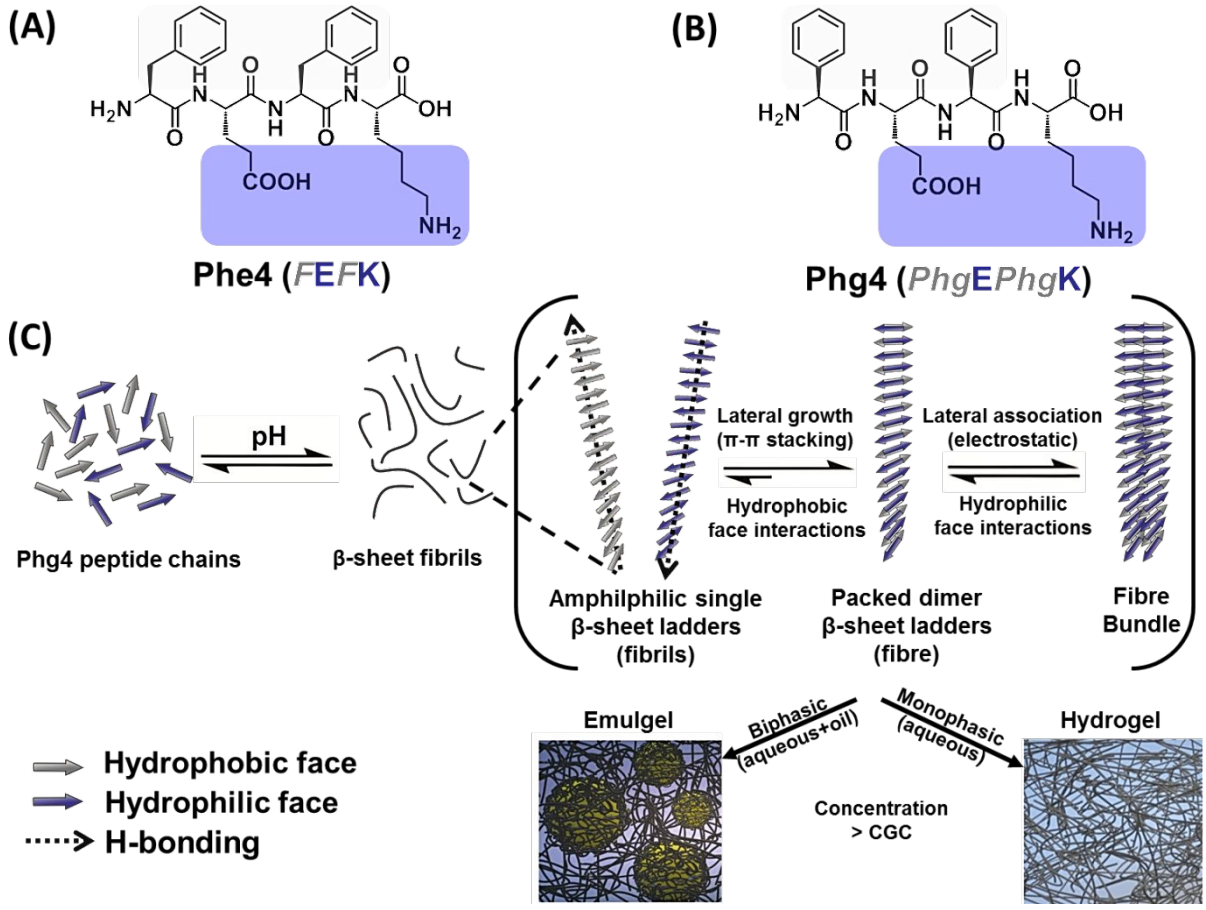

Figure 1: Molecular structures of A) Phe4 (*F*E*F*K) and B) Phg4 (*Phg*E*Phg*K) peptides. (*F* – phenylalanine, E – glutamic acid, K – lysine, *Phg* – phenylglycine). C) Schematic illustration of Phg4 self-assembly into the amphiphilic β-sheet single ladder form, though π-stacking of the aromatic rings alongside the intermolecular H-bonding between backbone amides. The single ladder form is in equilibrium with the more thermodynamically stable packed β-sheet ladders in aqueous medium, where the latter is formed by lateral growth through hydrophobic interactions of the aromatic rings projecting from the hydrophobic face. In monophasic medium, the packed form is more abundant forming nanofibres, which above critical gelation concentration (CGC) entangle into a nanofibous network forming hydrogels. In oil-water biphasic media, the amphiphilic single ladder will adsorb on the oil-water interface forming oil-in-water (O/W) emulgel. The hydrophobic face is denoted by grey colour and the hydrophilic by violet.

Materials and Methods

Materials. The Phe4 (*F*E*F*K) and Phg4 (*Phg*E*Phg*K) peptides were purchased from Cambridge Reagents Ltd. with ~>95% purity as estimated by HPLC (Figure S1). Melissa oil was acquired from Essential Oils Direct Ltd. Sodium Dodecyl Sulfate (SDS), sodium chloride, potassium phosphate monobasic, and potassium thiocyanate were purchased from Acros Organics with a purity of ≥99%. Potassium chloride was procured form Alfa Aesar. Polysorbate 80 (Tween 80) (99%), poly(ethylene glycol)-block-poly(propylene glycol)-block-poly(ethylene glycol)/poloxomer (Pluronic F-68) (99%) and alkyltrimethylammonium

bromide (cetrimide) (≥95%) were obtained from Sigma-Aldrich. HPLC grade water and chloroform were supplied by Thermo Fisher.

Computational Details. Initial models of single chain Phg4 and an anti-parallel amphiphilic packed dimer β-sheet ladder model composed of 16 Phg4 peptide chains (2×8) were built using Maestro and Protein Preparation Wizard,[20] with the protonation states assigned on the basis of PROPKA[21] at pH 7.0. To design these initial models, the solved structure of an amyloid forming peptide KLVFFA from amyloid beta (PDB code 3OW9) was used as a scaffold for editing to Phg4. Different alignments and conformations of the phenyl sidechains were manually explored in terms of the potential association between the two sheets in the packed dimer, considering favourable π-stacking distances and non-polar C-C, C-H and H-H van der Waals distances that are in the attraction region.[22,23] Prime v4.5[20] minimizations and sidechain predictions were performed on the starting models.[24] For the latter, rotamer libraries were used for random sidechain adjustments together with minimizations, until the sidechain rotamers were converged. The OPLS3 forcefield was used and water solvation effects accounted for using the implicit variable-dielectric generalized Born model (VSGB), which incorporates residue dependent effects.[25,26] Single chain Phg4 and the packed dimer model of Phg4 then underwent Desmond v4.7[20,27] 100 ns MD simulations in the NPT ensemble again with the OPLS3 forcefield but water solvation effects now explicitly accounted for using the TIP3P model. Three independent MD simulations were performed for the packed dimer using different seeds for assignment of the initial velocities and the trajectory post-processed packed-dimer energies, again using Prime. Full details of the simulations and post-processing are given in the Supporting Information. Following the dynamics, single chain and peptide aggregation geometries from the trajectories (3 simulations combined for the packed dimer) were clustered into the recommended number of clusters (20 and 31 for single chain and packed dimer, respectively) based on atomic RMSDs (heavy atoms) and the affinity propagation method.[28] The representative structures from each group were then considered in SQM PM7 optimizations using a restricted Hartree-Fock (RHF) wavefunction and molecular mechanics correction to CONH bonds (MMOK setting).[29] All optimizations included the COSMO implicit solvation model (COnductor-like Screening MOdel) with a dielectric constant of 78.4 for water.[30,31] The Localized Molecular Orbitals method available in MOPAC in the form of the linear scaling SCF MOZYME algorithm was used to speed up calculations.[32,33] Models with the lowest heats of formation were considered for further analyses. The SQM calculations were performed using MOPAC2016.[34]

Preparation of Hydrogels. Peptide powder was dissolved in HPLC water under vortex at 2500 rpm for 1 minute. To trigger self-assembly and gelation the pH was then adjusted to ~ 4.5-5 by stepwise addition of 0.5 M NaOH solution, whilst agitation for 30-60 seconds in between additions. After pH adjustment, the final volume was corrected using HPLC water to obtain the required concentration. Hydrogels were left in fridge at 4 °C overnight to equilibrate and used the following day.

Preparation of Emulsions and Emulgels. The oil phase (either chloroform or Melissa) was added dropwise to the peptide aqueous phase of pH values pre-adjusted separately to ~2, 4.5-5 or 8.6 (by stepwise addition of 0.5M NaOH solution as detailed under preparation of hydrogel), with mixing for 30 seconds in between additions at 2500 rpm using vortex. Different volumes of the oil phase were added to obtain W:O volume ratios of 2:8, 7:3, 6:4, 5:5, 4:6, 3:7 and 8:2.

Stability Testing of Emulsions and Emulgels. The stability of the emulgels with Melissa oil phase (EMG-M) formulation was compared with the traditional surfactants; SDS, poloxomer

(Pluronic F-68), cetrimide and Tween 80 all used at 50 mM and W:O ratio of 7:3. Three different conditions were investigated; long term stability (5 weeks), thermostability at 60 °C for 3 hours (in a Gallenkamp Hotbox oven with fan) and salt-stability using sodium chloride, potassium phosphate monobasic, and potassium thiocyanate salts at 100 mM for 1 week. For the perpetration of formulations for salt-stability the peptide and surfactants were dissolved straight into the salt solutions instead of HPLC water. Additionally, the long-term stability (10 weeks) of EMG-M with different W:O volume ratios (2:8, 3:7, 4:6, 5:5, 6:4, 7:3 and 8:2) at a peptide concentration of 30 mg/mL was examined. With the exception of the thermostability analysis all gels were incubated at room temperature (25 °C).

Attenuated Total Reflectance−Fourier Transform Infrared Spectroscopy (ATR-FTIR). Hydrogels and EMGs preparations were spread onto the crystal of a Thermo Nicolet IR200 spectrophotometer to evaluate the peptide secondary structure. Transmittance was recorded between 4000 and 400 cm^{-1} at 128 scans with resolution of 2 cm^{-1}. HPLC water was used as background, which was automatically subtracted from the sample spectra by OMNIC software provided with the instrument.

Fluorescence Thioflavin T (ThT) assay. ThT assay was performed using fluoroSENS spectrofluorometer (GILDEN photonics). ThT was mixed in 20 mg/mL of both peptide solutions/hydrogels during their preparation with a final 5 μM concentration and these were either left at the pH before titration (with their pH measured as ~2-2.3) or titrated using 0.5 M NaOH to a pH value of 4.5. Excitation wavelengths used were 400 nm and 450 nm and the fluorescence scan range was set to 460 nm – 600 nm.

Oscillatory Rheology. A stress-controlled Discovery Hybrid Rheometer HR-2 (TA instruments) was used to measure the rheological properties of the hydrogels and EMGs using a 20 mm Peltier plate with a parallel plate geometry and equipped with solvent trap to minimise evaporation. A sample of 500 μL was loaded onto the stage with the gap set to 250 μm from the upper plate. Any excess material was carefully removed using a spatula and the sample was left for 2 minutes to equilibrate at 37 °C. The amplitude sweep had already been carried out prior to determine that the linear viscoelastic region (37 °C, 1Hz and strains of 0.04 – 4%), which was then used to fix the strain of 0.2%. All radial frequency sweeps were carried out between 0.01 and 15 Hz and at a strain of 0.2%. Measurements were repeated in triplicates.

To examine stress recovery, time sweeps were carried out on the 40 mg/mL EMG-$M_{7:3}$ to simulate injection shear strain. Strain sweeps were measured at 0.2% for 5 min, followed by 1000% strain for 1 min as a simulation for injection strain, followed by 0.2% strain for 5 min, all carried out at 1Hz frequency.

Fluorescence Microscopy. The chloroform-in-water emulsion droplets were imaged by EVOS FL fluorescence microscope, where images were taken by EVOS X20 dry objective. For FITC fluorophore, excitation λ_{max} 490 nm was applied and emission λ_{max} 525 nm.

Scanning Electron Microscopy (SEM). A JCM-6000Plus Neoscope benchtop SEM was used to characterise network topology of the hydrogels as well as image the nanofibrillised microspheres formed within the EMGs. The peptide gel/emulgel was diluted 10-fold using HPLC water before mounting onto carbon disc, which was then either dried under vacuum or was left over night to air dry and sputter-coated with thin gold coating (10nm) before imaging.

Atomic Force Microscopy (AFM). Peptide samples were diluted from hydrogels and emulgels using ddH_2O to range of concentrations (0.025 mg/mL to 0.5 mg/mL). 10 μL of each

dilution was dropped onto freshly cleaved mica. After 2 min. excess solution was removed and the surface was washed once with 1 mL of HPLC grade H_2O. Excess water was then removed once again by wicking using Whatman No.1 filter paper. The samples were allowed to air-dry for one night prior to imaging. Areas of interest were imaged by scan assist mode in air using a Bruker Multimode 8 atomic force microscope with a Nanoscope V controller operating under Nanoscope v8.15 software. Imaging was performed using ScanAsyst Air tips. These silicon nitride probes with Al coating have a nominal radius of curvature of about 2 – 5 nm and a nominal spring constant of 0.4 N m^{-1} (Bruker AXS S.A.S, France). Height images with scan sizes of 2 μm × 2 μm were captured at a scan rate of 0.977 Hz and at a relative humidity of <40%. The instrument was periodically calibrated using a grating with 180 nm deep, 10-mm^2 depressions. Data was second-order flattened using the Nanoscope Analysis (v1.4) software prior to image export.

Transmission Electron Microscopy (TEM). A Thermo Scientific Tecnai G2 BioTwin TEM equipped with a high resolution Orius CCD SC1000 camera was used to characterise the fibre morphology of the hydrogels and EMGs at 100keV. Samples were diluted 10 folds using HPLC grade water. A 10 μL sample was adsorbed onto the carbon coated face of the copper grid (400 mesh), after 10 seconds it was blotted away using filter papers. The grid was then washed using 10 μL of water and finally negatively stained with 10 μL solution of 4% (w/w) uranyl acetate. After 4 days the samples were analysed after completely dried.

Small Angle X-ray Scattering (SAXS). SAXS experiments were performed on beamline I22 at the Diamond Light Source (DLS) facility in Didcot, UK. The energy of the beam was 12.4 keV corresponding to the X-ray wave length of 0.1 nm. Quartz capillaries (1.5 mm outer diameter, 0.01 mm wall thickness) were supplied from the Capillary Tube Supplies Ltd. 20 mg/mL of Phg4 hydrogel was introduced to capillaries via syringe. Acquisition time was 1 second and the area pixel array detector used to collect SAXS data was Pilatus P3-2M (from Dectris). The distance between samples and the detector was fixed to 2.211 m, resulting in a momentum transfer vector range of 0.086 (nm^{-1}) < q < 7.76 (nm^{-1}) with $q = (4\pi/\lambda)sin(\theta/2)$, where θ is the scattering angle and λ the wavelength of incident photons. Calibration of the momentum transfer was performed using silver behenate powder. ddH_2O in a capillary was used as background and subtracted from all measurements, whilst the subtraction mask was created using glassy carbon. Data were reduced using the processing tools at DawnDiamond software suite. The 2D scattering photon patterns were integrated using azimuthal integration tool to obtain a 1D scattering patterns.

Results and Discussions

Self-assembly and gelation properties. A phenylglycine based ionic self-complementary tetrapeptide sequence (Phg4) was designed as a constrained analogue of the previously investigated phenylalanine tetrapeptide (Phe4) (Figure 1A and 1B).[8,9] Guilbaud *et al.* showed that the Phe4 sequence neither self-assembled into β-sheet nanofibers nor formed self-supported hydrogel, as would normally be expected with ionic self-complementary sequences based on Zhang designs.[8,9] Self-assembly and gelation were only achieved by the effect of thermolysin reverse hydrolysis of Phe4 into the octapeptide FEFKFEFK at concentrations 0.5 and 70 mg/mL, respectively.[8,9] Those findings imply that the sequence length is crucial for stability of the self-assembled β-sheet structures.

Here, the secondary structure of both Phe4 and Phg4 peptides was studied at different concentrations using ATR-FTIR at pH 4.5-5 (Figures 2A and 2B). As predicted from Guilbaud

et al. previous findings[8,9], the Phe4 did not show the tendency to self-assemble into β-sheet structures, instead, unstructured random conformation at all the investigated concentrations was observed, where all spectra showed strong broad peak between 1645-1640 cm^{-1} (Figure 2A).[35,36] Similarly, Phg4 spectra of 5 and 10 mg/mL solution samples showed unstructured conformation. However, 20, 30 and 40 mg/mL concentrations showed prominent peaks at 1624 and 1650 cm^{-1} indicating H-bonding between backbone amides, as well as 1524 cm^{-1} amide II band; corresponding to formation of an extended β-sheet conformation (Figure 2B). Strikingly, Phg4 peptide showed to form self-supported cloudy hydrogel at a critical gelation concentration (CGC) ~20 mg/mL (Figure 2C, top panel), which is consistent with the FTIR spectra (Figure 2B). On the other hand, Phe4 failed to form self-supported materials at the same concentration range (5-40 mg/mL) (Figure 2C, bottom panel) as it lacked structure and did not self-organised β-sheet structures (Figure 2A).

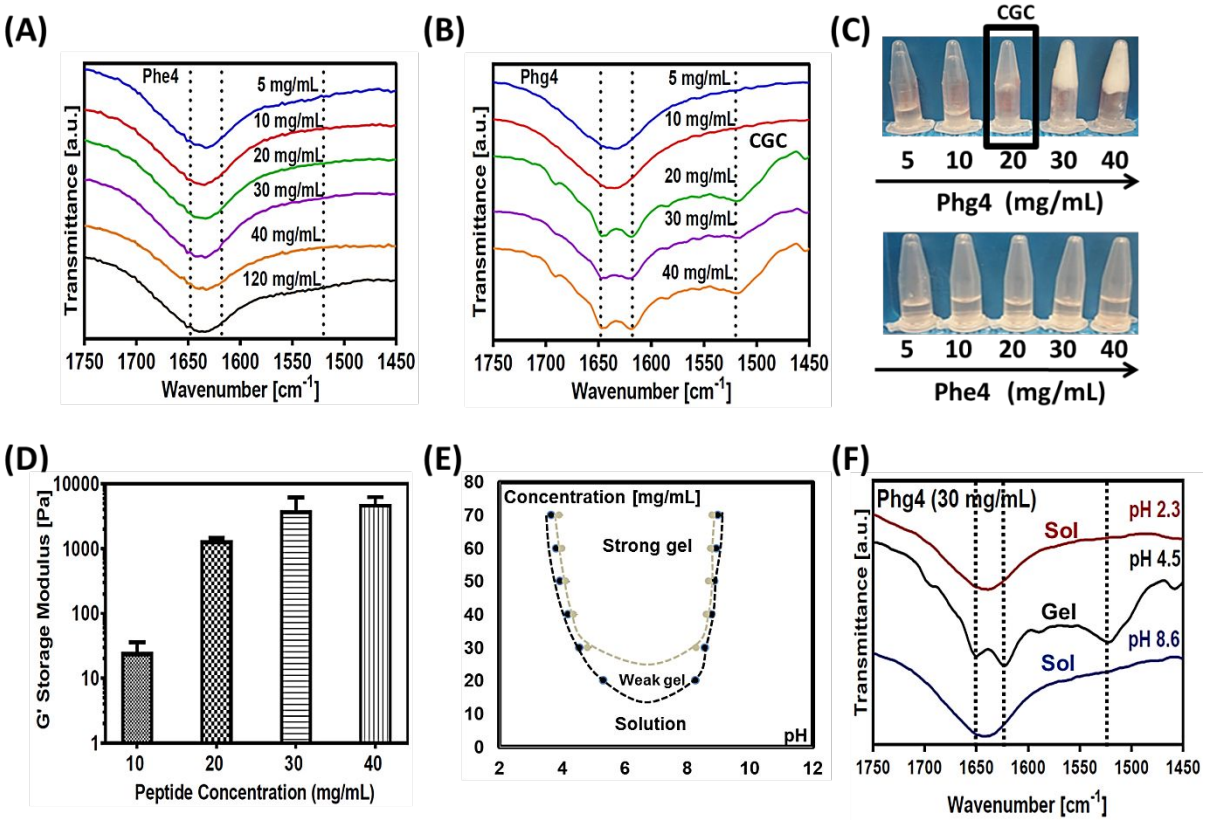

Figure 2: ATR-FTIR spectra for the two peptides: A) Phe4 and B) Phg4 at a series of concentrations. C) Inverted vial test of Phg4 (top panel) and Phe4 (bottom panel) peptides at pH 5. D) Shear modulus (G') (y axis set to log10) of Phg4 hydrogels at 6 rad s^{-1} obtained from the frequency sweep experiments performed at 0.2% strain. E) Phase diagram of Phg4 peptide as a function of pH and concentration. Three distinctive states were observed: strong gel, weak gel, and solution. F) ATR-FTIR spectra for Phg4 (30 mg/mL) showing phase transition from unstructured sol form at pH 2.3 to β-sheet gel form at pH 4.5 and back to unstructured sol form at pH 8.6.

The concentration dependency of Phg4 for the sol-gel transition and mechanical properties at pH 4.5-5 were investigated using shear rheometery. The shear moduli (G') significantly increased from ~ 40 Pa at 10 mg/mL to ~1350 Pa at 20 mg/mL and ~ 4500 Pa at 30 and 40 mg/mL (Figures 2D, S2A and S2B) showing the formation of self-supported viscoelastic hydrogels with CGC ~ 20 mg/mL confirming results from inverted vial test (Figure 2C, top panel), molecular conformations (Figure 2B) and phase diagram (Figure 2E). Materials of G' 1500 Pa or slightly below were thought to be weak gels, which are self-supportive and do not flow by effect of gravity in the inverted vial test, but can be forced to flow if the tube is strongly tapped. Gels of G' > 1500 Pa are strong gels and would not flow with tapping in the inverted

vial test (Figure 2E). In contrast, the shear moduli of Phe4 at the same concentrations and pH did not show the formation of stable viscoelastic hydrogel as observed from the very low shear moduli (G') values compared to Phg4 (data not shown).

Electrostatic interactions play a key role in the self-assembly and gelation properties of β-sheet forming peptides.[37] With this in mind, we have investigated self-assembly and sol-gel phase transitions as function of Phg4 peptide charge. To probe the charge status experimentally for comparison with theoretical calculations, peptide solution (30 mg/mL) was titrated using 0.5 M NaOH. The experimental titration curve indicates that the net peptide charge is neutral within pH range of 4.5-8 when compared to the theoretical charge curve (Figure S2C). Phase diagram of Phg4 hydrogel formation followed its symmetrical charge profile (Figures 2E and S2C) with strong hydrogels being formed at pH in the range ~4.5-8.5, shadowing the charge profile of Phg4 peptides of neutral net charge. This agrees with Caplan and co-workers results, which suggested that a reduction in electrostatic inter-molecular repulsion is required to enable stable molecular assembly of ionic self-complementary peptides.[37]

Remarkably, ATR-FTIR showed the structural switch of Phg4 from unstructured at pH 2.3 to β-sheet structure at pH 4.5 and back again to unstructured at pH 8.6, correlating well with the sol-gel-sol phase transitions and charge status, confirming that the gel formation is a result of the Phg4 self-assembly into β-sheet order (Figures 2E, 2F and S2C). Furthermore, fluorescence spectroscopy using Thioflavine T (ThT), which has strong binding affinity to β-sheet-like fibrils[38], has corroborated the conformational switch of Phg4 from unstructured at pH 2.3 to β-sheet order as indicated by the enhancement of ThT fluorescence intensity at pH 4.5, which was insignificant in case of Phe4, indicating the unique tendency of Phg4 to self-assembly (Figure S2D).

In silico modelling was exploited to help understand at the atomic level the observed propensity of Phg4 towards self-assembly, modelled as anti-parallel β-sheet ladders. Prime minimisation/sidechain predictions led to input models for single chain and packer dimer ladder Phg4 MD simulations. A 2 × 8 chain Phg4 dimer model was considered a good compromise between sheet length and accuracy, allowing us to post-process MD trajectory structures using theoretically more rigorous SQM PM7 calculations that better account for potential π-stacking interactions in the aggregated assembly. The packed dimer model maintained a stable aggregation structure for the full 100 ns simulation (3 independent simulations). The RMSD (system heavy atoms) was seen to stabilise after ~10-20 ns (Figure S3) and the last 80 ns of these simulations used for further analysis. In the models, hydrophobic phenyls from both sheets were intercalated limiting exposure to solvent, and the top-to-bottom aligned charged sidechains of hydrophilic K and E residues from consecutive chains formed a stable network of favourable ionic and hydrogen bond interactions throughout. The average number of inter-chain backbone hydrogen bonds over the three different packed dimer simulations was 2.7, 2.8 and 2.8 (overall average of 2.8). Each chain had stronger inter-chain hydrogen bonding on one side of the chain (averages of 3.5, 3.5 and 3.5 for the individual simulations; average when combined of 3.5) compared to the other (individual averages 1.7, 2.0 and 2.0; average when combined of 1.9). Generally at least 2 inter-chain hydrogen bonds were present throughout. We calculated an association energy for the propensity of single chains to aggregate into the models as ΔE_{assoc} (Eq. S1, Supporting Information) using the last 80 ns of each simulation with values of -540.3, -539.9 and -550.9 kcal mol^{-1} obtained, or an average ± standard deviation of -543.7±6.2kcal mol^{-1}, and indicative of significant stabilisation. A video presentation of the simulation with ΔE_{assoc}= -550.9 kcal mol^{-1} is included as Supporting Information. Despite the relatively good consistency of results, we highlight that

other models of aggregation are possible than these explored here and there are many possibilities (degrees of freedom) in terms of optimal π-stacking for the aggregated dimer. The PM7 optimization of the 31 trajectory cluster representatives allowed us to more closely analyse the nature of the phenyl interactions in the aggregated dimer, with the predicted most stable model based on the heats of formation shown in Figure 3A-C. The side-view (Figure 3A) demonstrates the formation of a hydrophobic inner core with phenyl rings from both sheets, and the network of hydrogen bonding involving K and E sidechains. The inter-chain backbone hydrogen bonds can also be seen but are more clearly visible in Figure 3B. Stacking and sandwich intercalation of the hydrophobic phenyl sidechains from the two sheets is evident when viewed from the top (Figure 3C) and includes T-stacking and parallel-displaced π-stacking interactions (Figure 3B). The anti-parallel chain arrangement allows the phenyl ring sidechains of non-terminal Phg residues (*Phg*E***Phg***K) from each chain to align forming a hydrophobic central core favourable for aggregation. Predicted stabilisation (from PM7/COSMO heat of formations) of the 16-chain Phg4 dimer model structure compared to free single peptide chains was considerable (-524.1 kcal mol^{-1}; relatively similar in magnitude to the ΔE_{assoc} values from the MD simulations), in further support of experiment and the packed aggregation of Phg4 chains in aqueous media. The stabilization values from PM7 optimizations can in fact be lower for other optimized frames from the MD simulations, with only MD cluster representatives used due to the computational expense involved.

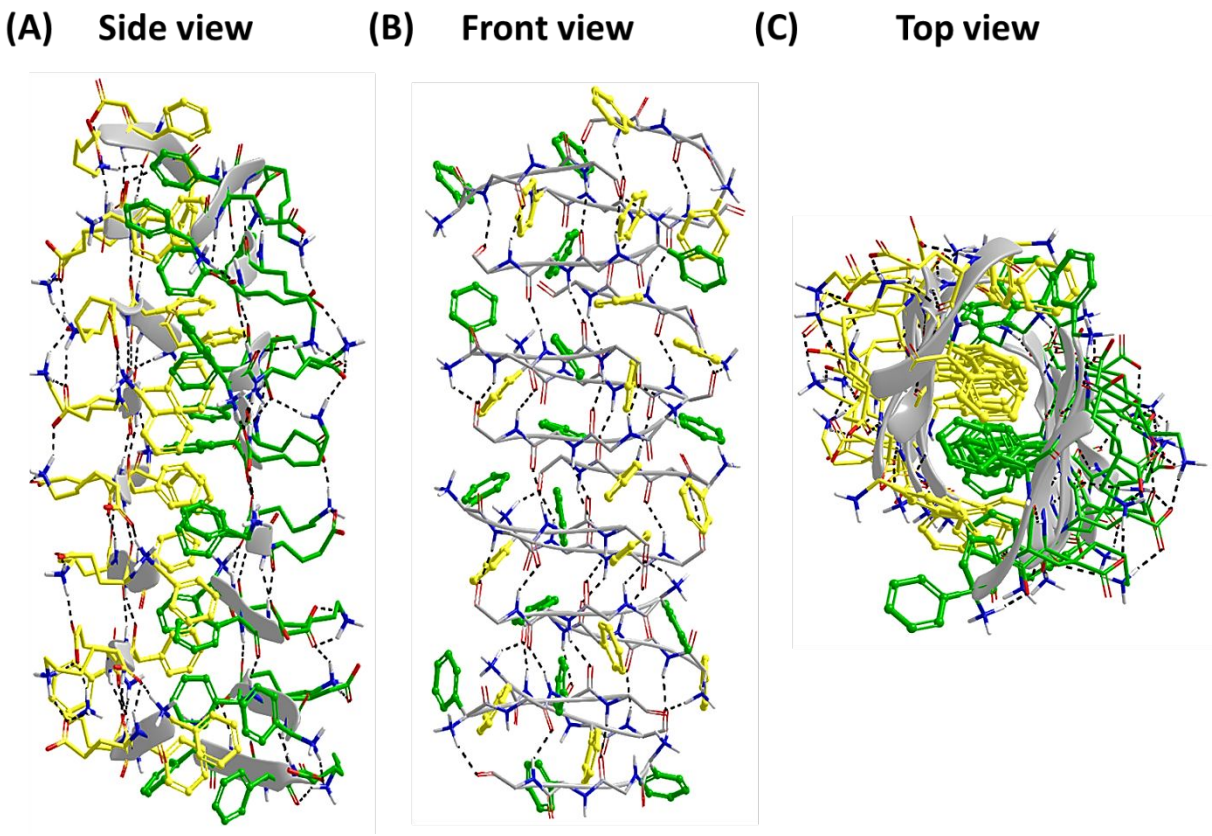

Figure 3: Predicted most stable packed dimer aggregation model from the PM7 calculations: A) side-view, B) front-view, with K and E sidechains omitted to more clearly demonstrate the inter-chain backbone hydrogen bonding and the phenyl ring stacking interactions and C) top-view. The RMSDs between the PM7 model and the model from the initial Prime side-chain predictions were 1.5 Å and 2.2 Å for backbone and sidechain, respectively, suggesting a good quality initial model from Prime but with PM7 theoretically more robust in terms of π-stacking optimization.[39]

On the mesoscopic scale, the ability of Phg4 peptide to form extended β-sheet nano-fibrillar structures was investigated using SEM, AFM and TEM. SEM showed a dense network of nano-fibrillar structures, which is typical for hydrogel formation (Figure 4A). The AFM micrograph clearly showed slightly twisted ribbon-like morphology, which stack in a hierarchal manner to form β-sheet fibrils (Figure 4B).[40] TEM showed relatively straight long entangled nano-fibres with Y-shaped branching, as well as lateral associations along the fibres length forming thicker bundles with sizes varied from ~7−11 nm (Figure 4C). Unlike Phg4, Phe4 samples did not show any nano-fibrillar structures when examined with the three microscopy techniques (data not shown).

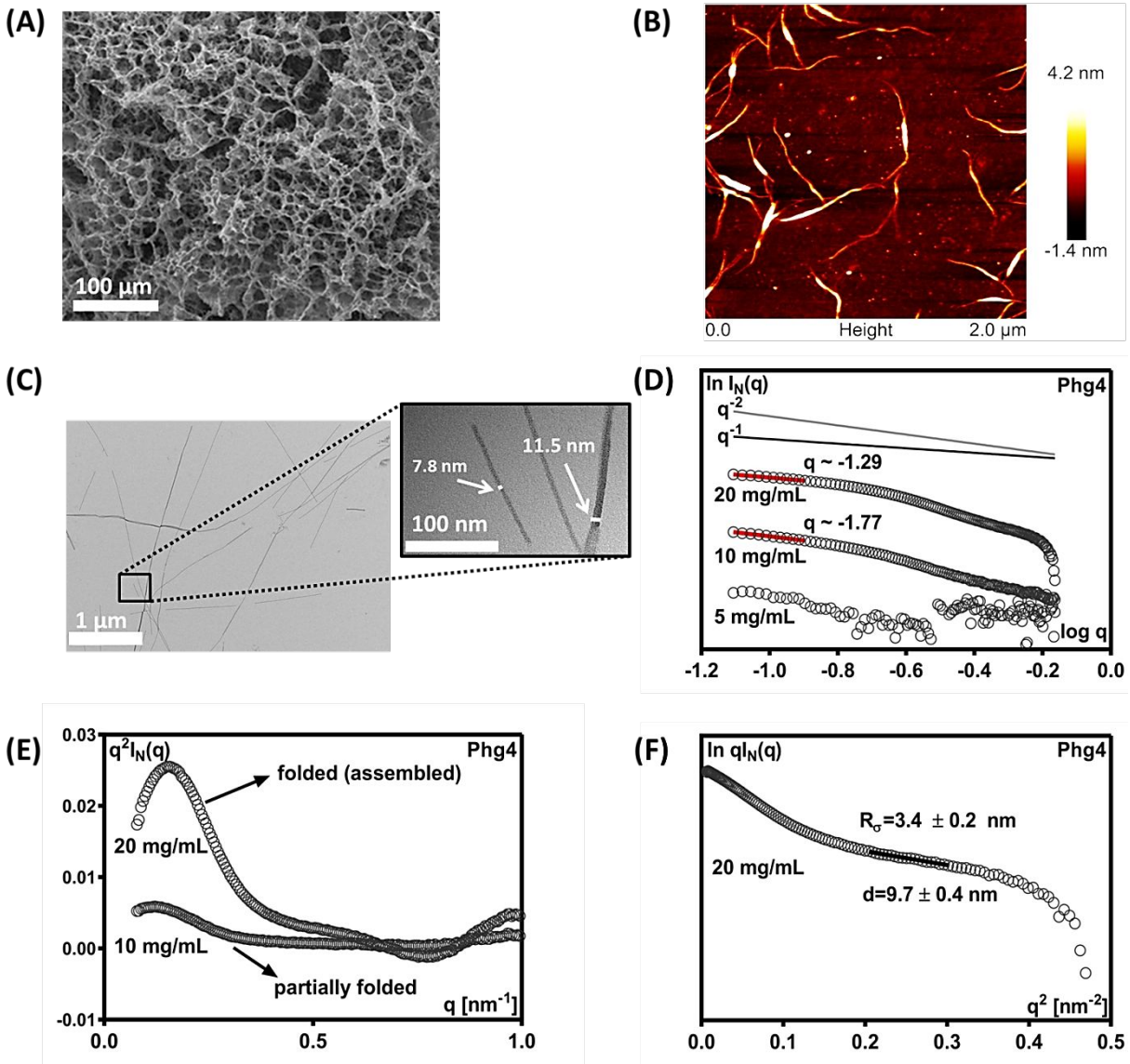

Figure 4: A) SEM image of 10X diluted and freeze-dried Phg4 hydrogel at 30 mg/mL. B) AFM micrographs of Phg4 hydrogel at 30 mg/mL diluted to 0.5 mg/mL. C) TEM micrographs of 10X diluted Phg4 hydrogel at 40 mg/mL, with arrows pointing to fibre bundles of ~7-11 nm size. D) *ln[$I_N(q)$] vs log q* representation of SAXS of 5, 10 and 20 mg/mL of Phg4. q^{-1} and q^{-2} behaviour are also presented. E) Kratky plot (q^2 $I_N(q)$ versus q representation) of 10 and 20 mg/mL Phg4. The curve shapes are marked by arrows corresponding to folded (assembled) and partially folded states. F) SAXS scattering pattern of a 20 mg/mL Phg4 at low q plotted in a *ln[qIN(q)]* versus q^2 representation.

SAXS was further used to investigate the formation and structure of the Phg4 nanofibres (Figure 4D-F). The *ln[I_N(q)] vs logq* representation indicated no fibre formation for 5 mg/mL, for which scattering similar to water level background was observed (Figure 4D). For 10 and 20 mg/mL samples, q values of ~-1.77 and 1.29 were obtained, respectively (Figure 4D). Typical ~ q^{-1} behaviour indicating rods and ~ q^{-2} indicating discs/flat objects were also plotted. As previously observed from FTIR measurements (Figure 2B), 10 mg/mL did not exhibit structured β-sheet peak. Likewise, SAXS confirmed that at this concentration Phg4 did not assemble into rod-like shape but random aggregates (q ~-1.77), whereas at 20 mg/mL rod-like objects closely resembling fibres were observed with q value 1.29; closer to q^{-1} behaviour. The slight deviation from the q~-1 behaviour of 20 mg/mL, is most likely coming from the tendency of Phg4 peptide to form flattened fibres and fibre bundles through inter-fiber lateral growth, as observed from AFM (Figure 4B) and TEM (Figure 4C), respectively. In fact, Kratky plots (*q^2[I_N(q)] vs. q*) for those two concentrations showed clear transition between partially folded at 10 mg/mL to fully folded (assembled) structures at 20 mg/mL (Figure 4E), respectively.[41] It has been previously shown that for rod objects (i.e. approximately fibres), for $qR_\sigma < 1.3$ (R_σ: cross-section radius of gyration) the scattering intensity can be written as[42,43]

$$\ln \boldsymbol{q\, I(q)} \propto -\frac{\boldsymbol{R_\sigma}^2}{\boldsymbol{2}}\boldsymbol{q^2} \quad \textit{Eq. 1}$$

If the scattering observed is of the form described by the above equation (1), then at low q a linear behaviour should be obtained in a *ln[qI_N(q)] vs. q^2* representation, which was the case with Phg4 (Figure 4F). The cross-section radius of gyration, R_σ, of the fibres can be estimated from the slope of the linear section. If the fibres can be modelled by an infinitely long cylinder, the R_σ is related to the diameter of the fibre, d, through the following equation:

$$R_\sigma = \sqrt{\frac{d^2}{8}} \quad \textit{Eq. 2}$$

By fitting of the linear region, the nano-fibre diameter size can be estimated as 9.7 ± 0.4 nm, which is in good agreement with the values obtained from TEM (Figure 4C). In contrary, Phe4 did not exhibit any fibril-like scattering patterns (data not shown).

The above discussed results clearly showed the unique tendency of the ultra-short constrained Phg4 sequence to adopt stable β-sheet conformation in a concentration-dependent and pH-responsive fashion, surpassing its Phe4 counterpart that failed to self-assemble into β-sheet structure. Interestingly, the seemingly minimal change in the chemical structure had large influence on the molecular stability of self-assembly for these tetrapeptide sequences (Figures 1A and 1B). This is attributed to the aromatic rings orientation in Phg4, which are directly attached to the peptide sequence backbone making them readily positioned for π-stacking stabilising the self-assembled structure alongside the H-bonds formed between backbone amides and the salt bridges between K and E residues sidechains; all together forming a very stable network of non-covalent interactions from top to bottom along the fibre axis (Figure 3).

Self-assembly and interfacial properties. Both Phe4 and Phg4 tetrapeptides are ionic self-complementary sequences with alternating hydrophobic and hydrophilic residue pattern (Figure 1A and 1B). The amphiphilic-like design suggests that both peptides can exhibit interfacial activity. To test this, the peptide aqueous phase (20 mg/mL) was mixed with chloroform as the immiscible oil phase in 1:1 volume ratio at a range of pH values. Strikingly, only Phg4 managed to form stable emulsion, but not Phe4 at pH5 (Figure 5A). Also, both peptides showed immediate phase separation after mixing at pH 2 and 8.5 (data not shown).

This implies that the surface activity is due to the adsorption of Phg4 amphiphilic nanofibers at the oil-water interface, which are formed at pH5, rather than the monomeric non-assembled peptide chains at pH 2 or 8.5 (Figure 2F). Phe4 failed to stabilise emulsions at all pH range as it does not self-assemble into amphiphilic β-sheet nanofibers. Fluorescence microscopy of Phg4 emulsion revealed the formation of oil-in-water (O/W) macroemulsion (~50-200 µm) with the continuous aqueous phase stained with Fluorescein Isothiocyanate (FITC) green fluorescence (Figure 5A).

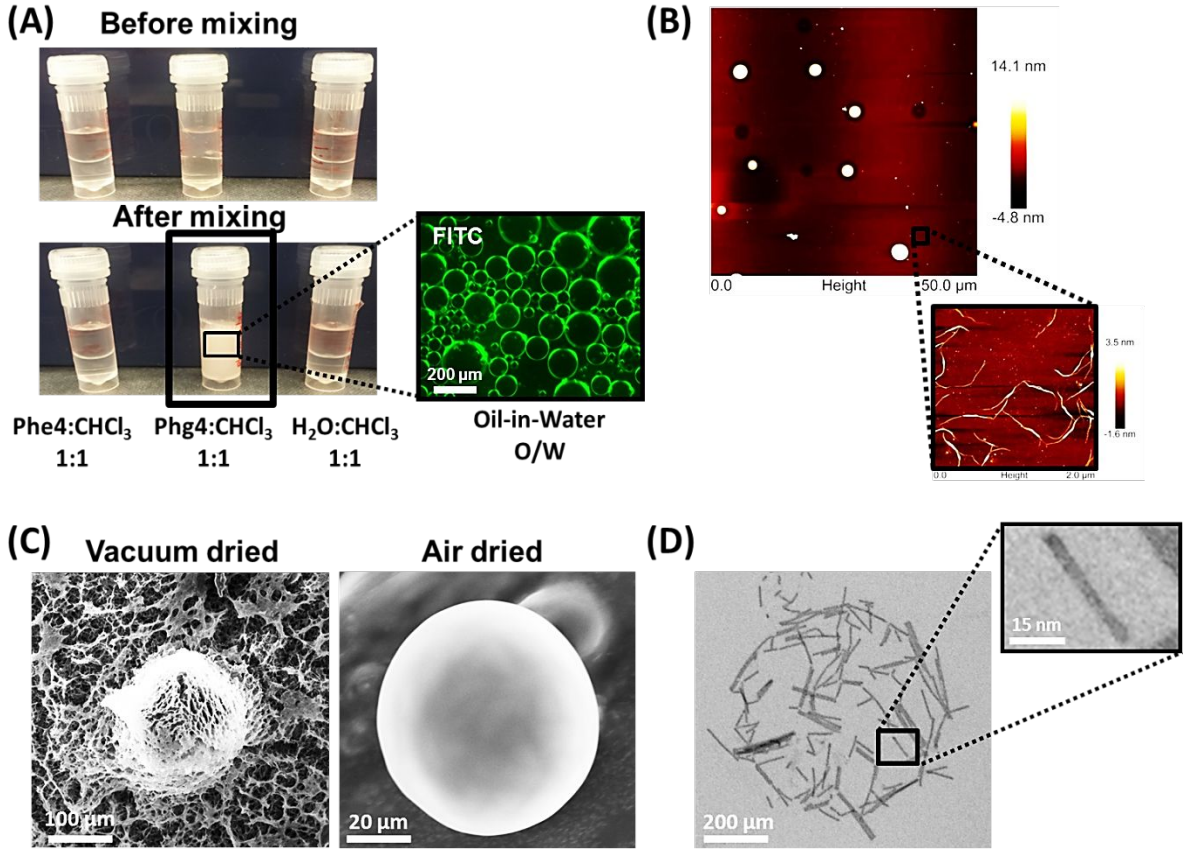

Figure 5: A) Photograph of 20 mg/mL Phe4 and Phg4 water chloroform ($CHCl_3$) mixtures at 1:1 volume ratio before and after mixing. Fluorescence microscopy image confirmed the formation of Phg4 oil-in-water (O/W) emulsion with the continuous aqueous phase stained with Fluorescein Isothiocyanate (FITC). B) AFM of Phg4-$CHCl_3$ emulsion showing microspheres formed at the oil-water interface at 1:1 volume ratio after sample drying. Background region close to the sphere shows individual fibrils similar to those observed in hydrogels (Figure 3B). C) SEM micrographs of a 30 mg/mL emulgel prepared at 1:1 W:O ratio, which has been 10X diluted and either vacuum dried (left) or air dried (right). D) TEM micrographs of 10X diluted Phg4 chloroform-in-water at 30 mg/mL, showing short fibre bundles of ~9 nm size arranged in a sphere like shape.

AFM of the dried sample revealed the formation of Phg4 microspheres surrounded with nanofibres (Figure 5B) similar to those forming hydrogels (Figure 4B), implying the formation of emulgels (EMG). This suggests that the amphiphilic nanofibrils formed of unpacked β-sheet single ladders are adsorbed at the surface of the oil phase (chloroform) with the Phg aromatic rings oriented towards chloroform and the hydrophilic E and K residues facing the aqueous phase, by this following the "oriented wedge theory" first suggested by Harkins and Keith in early 1900's (Figure 1C).[44,45] Based on the AFM micrograph, we also hypothesise that chloroform evaporation can lead to the formation of nanofibrillised hollow microspheres entangled within the nanofibrous network of the surrounding aqueous medium. Evidently, SEM micrograph of vacuum dried emulsion clearly showed the formation of nanofibrillised porous microspheres within the nanofibrous network of the continuous phase, while the air

dried sample showed the formation of solid peptide microspheres (Figure 5C). It is worth mentioning here that artefacts could happen from sample preparation, where it was observed that the nanofibrous network surrounding microspheres was slightly cracked from vacuum drying (Figure 5C, left micrograph). In general, Phg4 microspheres showed similar morphology in SEM to the Fmoc-YL that was previously reported by Ulijn and co-workers to stabilise chloroform-in-water emulsions,[16] as well as the surfactant like decapeptide A_9R that was reported by Hamley and co-workers to stabilise water-in-1-bromohexadecane emulsions.[19] The TEM micrograph of diluted emulsion manifested short β-sheet fibre bundles adopting spherical arrangement with bundle diameter size of ~ 9nm (Figure 5D), which is within the size range of the hydrogel forming fibres (Figures 4C and 4F).

Phg4 peptide emulgels (EMG). We have then changed the oil phase from chloroform to the pharmaceutically relevant and more viscous oil phase, Melissa oil, which is extracted from the leaves of Melissa officinalis species of the Lamiaceae family. It has been reported that Melissa oil possesses antimicrobial[46], antifungal[47], antiviral[48] and antioxidant[49] activities. The Phg4 based O/W emulgels with Melissa as the oil phase (EMG-M) has been formulated by simple mixing of oil droplets in the peptide aqueous phase at self-assembly pH 5. First, the effect of Phg4 peptide concentration on the formulation stability was studied at 1:1 W:O ratio. No emulsion formation was observed at 10 mg/mL, but at 20 mg/mL emulsions were obtained with minimal phase separation observed at concentrations ≥ 30 mg/mL (Figure 6A). This correlates with the FTIR spectra, where Phg4 was unstructured at 10 mg/mL, and acquired the β-sheet structure at 20 mg/mL, where self-assembly into the emulsifying amphiphilic β-sheet ladders occurs (Figure S4A).

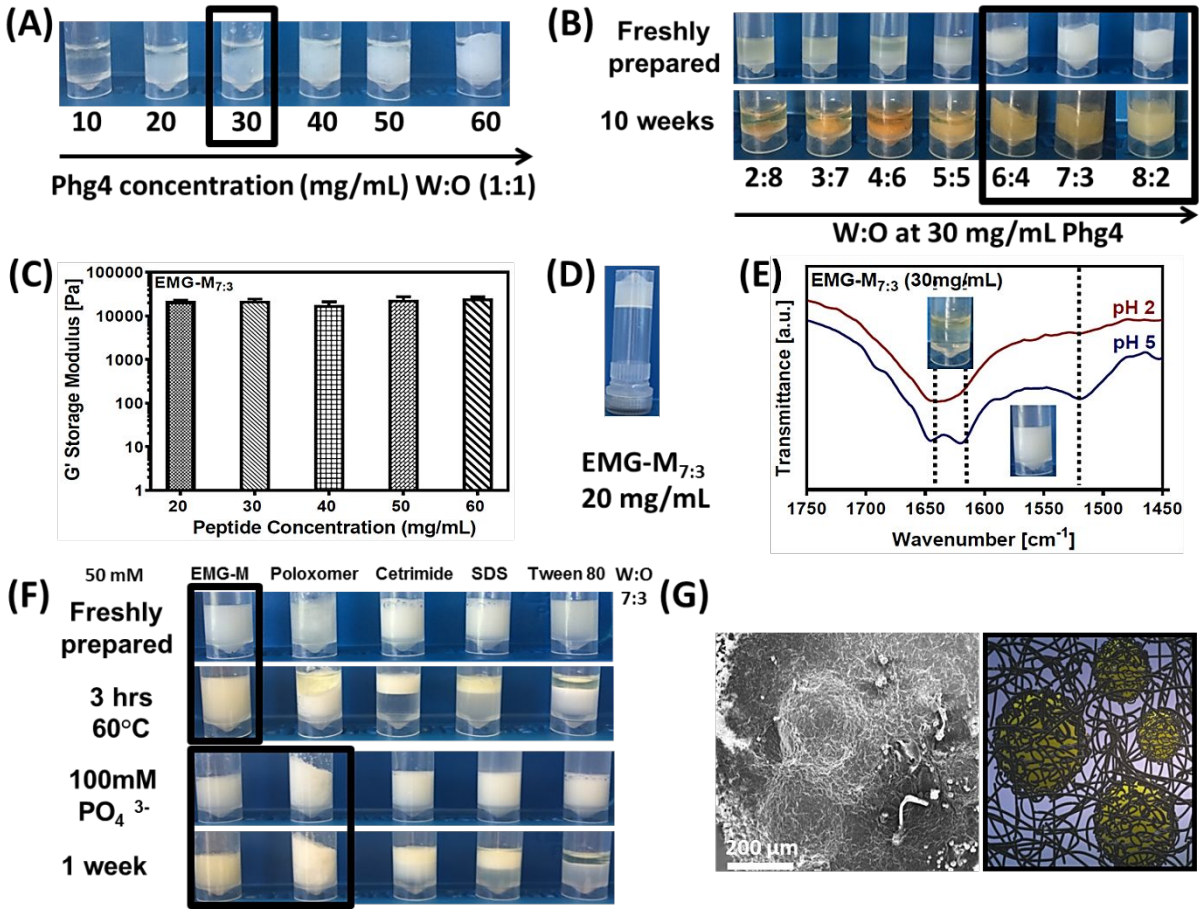

Figure 6: A) A series of Phg4 Melissa oil mixtures with a range of peptide concentrations (10-60 mg/mL) at 1:1 W:O volume ratio. B) EMG-M (30 mg/mL) mixed at a range of different W:O volume ratios (2:8-8:2) tested for phase separation over 10 weeks at room temperature. C) Shear moduli (G') of EMG-$M_{7:3}$ at a range of peptide concentrations (20-60 mg/mL), performed at 6 rad s^{-1} obtained from the frequency sweep experiments performed at 0.2% strain D) Inverted vial test of EMG-$M_{7:3}$ (20 mg/mL) at pH 5. E) ATR-FTIR spectra of EMG-$M_{7:3}$ (30 mg/mL) showing phase transition from unstructured immiscible form at pH 2to β-sheet structured emulgel form at pH 5 F) Emulsion stability profiles of EMG-$M_{7:3}$ versus poloxomer (Pluronic F-68), cetrimide (alkyltrimethylammonium bromide), sodium dodecyl sulphate (SDS) and tween 80 at 50mM emulsifier concentration after incubation for 3hrs at 60°C (top panel) and after incubation with 100mM potassium phosphate monobasic for 1 week (bottom panel). G) Left: SEM image of EMG-$M_{7:3}$ (30 mg/mL), which has been 10X diluted and vacuum dried, showing two oil droplets stabilized by peptide fibrous network at the interface. Right: illustration of the O/W EMG-M showing the Melissa oil droplets in yellow entrapped within the peptide nanofibrous network suspended in the continuous aqueous hydrogel phase in blue.

The effect of W:O ratio on the formulation stability was evaluated at 30 mg/mL peptide concentration. After 10 weeks of storage, we noticed that increasing water volume above 50% yielded the most stable formulations (Figure 6B). Indeed, FTIR spectroscopy confirmed these visual observations with strong β-sheet peak at ~ 1624 cm^{-1} for W:O ratios 6:4, 7:3 and 8:2 (Figure S4B). Shear rheology confirmed the formation of viscoelastic hydrogel-like system for W:O 7:3 samples at a range of peptide concentrations (20-60 mg/mL) with shear moduli ~ 20kPa (Figures 6C, S5A and S5B). The high stiffness of EMG-M, as indicated from G' values, compared to hydrogels of G' hundreds Pa (Figures 2D and S2B) could be attributed to network structure changes associated with the formation of nanofibrillised microspheres; which could have enhanced the mechanical strength of the nanofibrous network of the continuous aqueous phase. The EMG-M stiffness was not significantly affected by the W:O ratio (Figure S5C). Also, EMG-M formulation showed to be not only shear-thinning but also pseudoplastic thixotropic, where instantaneous, but partial recovery from shear strain was observed from the controlled strain profile of EMG-$M_{7:3}$ at 40 mg/mL Phg4 concentration (Figure S5D). This implicates the injectability of these peptide emulgels (Figure S5D), where fast recovery kinetics is a desirable parameter to avoid uncontrolled release of cargos post injection; which is a useful material property for drug and cell delivery applications. Inverted vial test revealed a CGC for a self-supported emulsion-gel or "emulgel" (EMG) system of ~ 20 mg/mL for 7:3 W:O ratio (Figure 6D), similar to that observed for the hydrogel formulations (Figure 2C, top panel).

The stability profile of EMG-$M_{7:3}$ (30 mg/mL) formulation was studied under various physical, chemical and environmental conditions. The EMG-M stability was indeed affected by pH, where the colloidal system was most stable at the self-assembly pH 5 due to the formation of the emulsifier amphiphilic β-sheet ladders (Figure 6E). Phase separation was observed at pH 2 (Figure 6E) and 8.5 (data not shown), as the peptide is unstructured at these pH values (Figures 2F and 6E). The correlation of structural and phase transitions suggests that the amphiphilic nanofibres are the effective emulsifier and not the non-assembled individual peptide chains. Over long storage (up to 5 weeks), EMG-M showed to be more stable, compared to a variety of commercial surfactants belonging to different classes of surface active agents and commonly used in pharmaceutical and cosmetic products such as the cationic surfactant cetrimide (alkyltrimethylammonium bromide), the anionic sodium dodecyl sulphate (SDS) and the non-ionic tween 80 that all showed phase separation when used at same concentration (50mM) (Figure S6A). However, only the non-ionic surfactant poloxomer (Pluronic F-68) showed similar stabilisation as EMG-M, as both formed self-supported hydrogel that helped stabilising suspended oil droplets through the highly viscous continuous phase (Figure S6A). EMG-M was the only formulation that showed thermal stability when heated for 3hrs at 60°C, while phase separation occurred with all other emulsifiers including poloxomer (Figure 6F, top panel). Salting out effect was studied as well using a variety of salts (phosphate, chloride and thiocyanate), and in all cases only EMG-M and poloxomer emulsions showed to be stable

(Figure 6F bottom panel and Figure S6B). Ulijn and co-workers have also reported the ability of the β-sheet forming Fmoc capped short aromatic sequences to stabilise chloroform-in-water emulsions for 24 hours better than SDS when incubated with phosphate, chloride and thiocyanate salts.[16]

SEM of diluted EMG-M showed peptide nanofibrils adsorbed at the oil-water interface and surrounding the oil droplets (Figure 6G, left panel). This confirms the stabilisation of the EMG system through formation of amphiphilic nanofibres that not only adsorb at the oil-water interface, but also form a fibrous network that help stabilising the system by entrapping the suspended oil droplets within the highly viscous hydrogel continuous phase (Figure 6G, right panel).

Our results, therefore, have demonstrated the considerable potential of using Phg4 amphiphilic nanofibres as emulsifiers in pharmaceutical, cosmetics and food industry, as it overcomes the major limitation of commercial surfactants; the instability towards environmental and storage conditions.

Conclusion

To the best of our knowledge, we have reported for the first time the shortest ionic self-complementary sequence (Phg4 tetrapeptide) that self-assembles into stable amphiphilic β-sheet nanofibres capable of gelation and emulsification. This was achieved by the rational design of a constrained tetrapeptide analogue of the previously reported non-assembling Phe4, exploiting the properties of a more rigid phenylglycine residue. We hypothesized the atomistic interactions leading to stability of self-assembled fibrils through hybrid molecular dynamics simulations and SQM calculations, which highlighted the strong potential for favourable aggregation through π-stacking interactions involving the aromatic Phg sidechains from different sheets. These fibrils showed both the ability to form hydrogels in monophasic aqueous medium and interfacial activity in biphasic media forming stable emulgels. Our results highlight the importance of complementary inter-facial non-covalent forces alongside backbone amide hydrogen bonding to stabilise the molecular self-assembly of short peptides as exemplified by favourable aromatic stacking in this study. Ultra-short Ionic-complementary Constrained Peptides or UICPs have significant potential for the development of cost-effective, sustainable and multifunctional soft nanomaterials based on robust nano-assemblies possessing both hydrogelation and emulsification properties; beneficial attributes for the development of a wide range of materials for biomedical, pharmaceutical, cosmetic and food applications.

Acknowledgments

The authors are grateful to the School of Pharmacy and Biomedical Sciences at University of Central Lancashire (UCLan) for funding this work through the start-up fund awarded to MAE and the Graduate Internship awarded to JL. Authors are grateful to the staff in JB Firth analytical suite at UCLan for their assistance and training RP and JL on how to use SEM. Authors also acknowledge the Engineering and Physical Sciences Research Council (EPSRC) for supporting the work of JKW of the Northwest Nanoscience Doctoral Training Centre (NOWNANO DTC), with an EP/G03737X/1 grant, and an EPSRC doctoral training award (DTA) from the School of Materials, University of Manchester. Authors would like to thank the staff in the EM facility in the Faculty of Biology, Medicine and Health, of the University of Manchester (UoM), for their assistance, and the Welcome Trust for equipment grant support to the EM facility. The authors are grateful to Dr Nigel Hodson (UoM) for his assistance with the AFM experiments, Xinyi Zhu (UoM) for training RP on TEM sample preparation and

Diamond Light Source for beam time award (SM17102) to MAE and JKW and the staff on beamline I22 for their support with the SAXS experiments, in particular Andrew Smith. Authors would also like to thank Nadia Moinuddin (UCLan) for acquiring preliminary data on chloroform-in-water emulsions funded by UCLan Undergraduate Research Internship Scheme (URIS).

Notes

The authors declare no competing financial interest. All research data supporting this publication are directly available within this publication and associated supporting information.

ORCID numbers of authors

Jacek K. Wychowaniec: https://orcid.org/0000-0002-6597-5242
Vikesh Chhabria: https://orcid.org/0000-0001-7812-7368
Yogita Patil-Sen: https://orcid.org/0000-0002-4286-8874
Araida Hidalgo--Bastida: https://orcid.org/0000-0003-2652-2395
Joseph M. Hayes: https://orcid.org/0000-0002-7745-9616
Mohamed A. Elsawy: http://orcid.org/0000-0003-3964-2150

Supplementary information

The supplementary information is available free of charge via the Internet at XYZ.

Molecular dynamics details, HPLC chromatograms of used peptides, additional oscillatory rheology data for hydrogels and emulgels (strain sweep, frequency sweep and strain recovery), theoretical net charge and titration curve of Phg4 peptide, ThT fluorescence for the two peptides, additional ATR-FTIR for emulgel EMG-M (different peptide concentrations and W:O ratios) and emulsion stability profiles for EMG-M compared to commercial emulsifiers. (PDF)

Molecular Dynamics simulation video for Phg4 packed dimer. (MP4)

References

(1) Mandal, D.; Shirazi, A. N.; Parang, K. Self-assembly of peptides to nanostructures. *Org. Biomol. Chem.* **2014,** *12* (22), 3544–3561.
(2) Panda, J. J.; Chauhan, V. S. Short peptide based self-assembled nanostructures: implications in drug delivery and tissue engineering. *Polym. Chem.* **2014,** *5* (15), 4418–4436.
(3) Zhang, S.; Lockshin, C.; Cook, R.; Rich, A. Unusually stable β-sheet formation in an ionic self-complementary oligopeptide. *Biopolymers* **1994,** *34* (5), 663–672.
(4) Zhang, S. G.; Holmes, T.; Lockshin, C.; Rich, A. Spontaneous assembly of a self-complementary oligopeptide to form a stable macroscopic membrane. *Proc. Natl. Acad. Sci. U. S. A.* **1993,** *90* (8), 3334–3338.
(5) Zhang, S.; Lockshin, C.; Herbert, A.; Winter, E.; Rich, A. Zuotin, a putative Z-DNA binding protein in *Saccharomyces cerevisiae*. *EMBO J.* **1992,** *11* (10), 3787–3796.
(6) Elsawy, M. A.; Smith, A. M.; Hodson, N.; Squires, A.; Miller, A. F.; Saiani, A., Modification of beta-sheet forming peptide hydrophobic face: effect on self-assembly and gelation. *Langmuir* **2016**, *32* (19), 4917–4923.

(7) Gao, J.; Tang, C.; Elsawy, M. A.; Smith, A.; Miller, A.; Saiani, A. Controlling self-assembling peptide hydrogel properties through network topology. *Biomacromolecules* **2017,** *18* (3), 826–834.
(8) Guilbaud, J.-B.; Vey, E.; Boothroyd, S.; Smith, A.M.; Ulijn, R.V.; Saiani, A.; Miller, A. F. Enzymatic catalyzed synthesis and triggered gelation of ionic peptides. *Langmuir* **2010,** *26* (13), 11297–11303.
(9) Guilbaud, J.-B.; Rochas, C.; Miller, A. F.; Saiani, A., Effect of Enzyme Concentration of the Morphology and Properties of Enzymatically Triggered Peptide Hydrogels. *Biomacromolecules* **2013,** *14* (5), 1403–1411.
(10) Yokoi H, Kinoshita T, Zhang S. Dynamic reassembly of peptide RADA16 nanofiber scaffold. *Proc. Natl. Acad. Sci. U. S. A.* **2005,** *102* (24), 8414–8419.
(11) Swanekamp, R. J.; DiMaio, J. T. M.; Bowerman, C. J.; Nilsson, B. L. Coassembly of enantiomeric amphipathic peptides into amyloid-inspired rippled β-sheet fibrils. *J. Am. Chem. Soc.* **2012,** *134* (12), 5556–5559.
(12) Bowerman, C. J.; Nilsson, B. L. Review self-assembly of amphipathic β-sheet peptides: Insights and applications. *Pept. Sci.* **2012,** *98* (3), 169–184.
(13) Lee, N. R.; Bowerman, C. J.; Nilsson, B. L. Effects of varied sequence pattern on the self-assembly of amphipathic peptides. *Biomacromolecules* **2013,** *14* (9), 3267–3277.
(14) Gazit, E. A possible role for π-stacking in the self-assembly of amyloid fibrils. *The FASEB J.* **2002,** *16* (1), 77–83.
(15) Li, J.; Du, X. W.; Hashim, S.; Shy, A.; Xu, B. Aromatic-Aromatic interactions enable alpha-helix to beta-sheet transition of peptides to form supramolecular hydrogels. *J. Am. Chem. Soc.* **2017,** *139* (1), 71–74.
(16) Bai, S.; Pappas, C.; Debnath, S.; Frederix, P.W.J.M.; Leckie, J.; Fleming, S.; Ulijn, R. Stable Emulsions Formed by Self-Assembly of Interfacial Networks of Dipeptide Derivatives. *ACS Nano* **2014**, *8* (7), 7005–7013.
(17) Moreira, I. P.; Sasselli, I. R.; Cannon, D. A.; Hughes, M.; Lamprou, D. A.; Tuttle, T.; Ulijn, R. V. Enzymatically activated emulsions stabilised by interfacial nanofibre networks. *Soft Matter* **2016**, *12* (9), 2623–2631.
(18) Aviño, F.; Matheson, A. B.; Adams, D. J.; Clegg, P. S. Stabilizing bubble and droplet interfaces using dipeptide hydrogels. *Org. Biomol. Chem.* **2017**, *15* (3), 6342–6348.
(19) Castelletto, V.; Edwards-Gayle, C. J. C.; Hamley, I. W.; Barrett, G.; Seitsonen, J.; Ruokolainen, J. Peptide-stabilized emulsions and gels from an arginine-rich surfactant-like peptide with antimicrobial activity. *ACS Appl. Mater. Interfaces* **2019**, *11* (10), 9893–9903.
(20) Schrodinger Release 2016-3, Schrodinger LLC, New York, NY, **2016**.
(21) Olsson, M. H.; Søndergaard, C. R.; Rostkowski, M.; Jensen, J. H. PROPKA3: Consistent treatment of internal and surface residues in empirical pKa predictions. *J. Chem. Theory Comput.* **2011,** *7* (2), 525–537.
(22) McGaughey, G. B.; Gagne, M.; Rappe, A. K. π-stacking interactions alive and well in proteins. *JBC* **1998,** *273* (25), 15458–15463.
(23) Hayes, J. M.; Greer, J. C.; Morton-Blake, D. A. A force-field description of short-range repulsions for high density alkane molecular dynamics simulations. *J. Comp. Chem.* **2004,** *25* (16), 1953–1966.
(24) Jacobson M. P.; Friesner, R. A.; Xiang, Z.; Honig, B. On the role of the crystal environment in determining protein side-chain conformations. J. Mol. Biol. **2002,** *320* (3), 597–608.
(25) Harder, E.; Damm, W.; Maple, J. Wu, C.; Reboul, M.; Xiang, J. Y.; Wang, L.; Lupyan, D.; Dahlgren, M. K.; Knight, J. L.; Kaus, J. W.; Cerutti, D. S.; Krilov, G.; Jorgensen, W. L.; Abel, R.; Friesner, R. A. OPLS3: A Force Field Providing Broad Coverage of Drug-like Small Molecules and Proteins. *J. Chem. Theory Comput.* **2016,** *12* (1), 281–296.

(26) Li, J.; Abel, R.; Zhu, K.; Cao, Y.; Zhao, S.; Friesner, R. A. The VSGB 2.0 model: a next generation energy model for high resolution protein structure modelling. *Proteins* **2011,** *79* (10), 2794–2812.
(27) Desmond Molecular Dynamics System, D. E. Shaw Research, New York, NY, **2016**.
(28) Frey, B. J.; Dueck, D. Clustering by passing messages between data points. *Science* **2007,** *315* (5814), 972–976.
(29) Stewart, J. J. P. Optimization of parameters for semiempirical methods VI: more modifications to the NDDO approximations and re-optimization of parameters. *J. Mol. Model.* **2013,** *19* (1), 1–32.
(30) Klamt, A.; Schüürmann, G. COSMO: a new approach to dielectric screening in solvents with explicit expressions for the screening energy and its gradient. *J. Chem. Soc., Perkin Trans. 2* **1993,** *2* (5), 799–805.
(31) Klamt, A.; Moya, C.; Palomar, J. A comprehensive comparison of the IEFPCM and SS(V)PE continuum solvation methods with the COSMO approach. *J. Chem. Theory Comput.* **2015,** *11* (9), 4220–4225.
(32) Høyvik, I.-M.; Jansik, B.; Jørgensen, P. Trust region minimization of orbital localization functions. *J. Chem. Theory Comput.* **2012,** *8* (9), 3137–3146
(33) Lehtola, S.; Jónsson, H. Unitary optimization of localized molecular orbitals. *J. Chem. Theory Comput.* **2013,** *9* (12), 5365–5372.
(34) MOPAC2016, Version 18.270L, James J. P. Stewart, Stewart Computational Chemistry, website: http://OpenMOPAC.net.
(35) Barth, A. Infrared spectroscopy of proteins. *BBA – Bioenergetics* **2007,** *1767* (9), 1073−1101.
(36) Barth, A.; Zscherp, C. What vibrations tell us about proteins. *Q. Rev. Biophys.* **2002,** *35* (4), 369−430.
(37) Caplan, M. R.; Moore, P. N.; Zhang, S. G.; Kamm, R. D.; Lauffenburger, D. A., Self-assembly of a beta-sheet protein governed by relief of electrostatic repulsion relative to Van der Waals attraction. *Biomacromolecules* **2000,** *1* (4), 627−631.
(38) Maskevich, A. A.; Stsiapura, V. I.; Kuzmitsky, V. A.; Kuznetsova, I. M.; Povarova, O. I.; Uversky, V. N.; Turoverov, K. K., Spectral properties of thioflavin t in solvents with different dielectric properties and in a fibril-incorporated form. *J. Proteome Res.* **2007**, *6* (4), 1392−1401.
(39) Yilmazer, N. D.; Korth, M. Enhanced semiempirical QM methods for biomolecular interactions. *Comput. Struct. Biotechnol.* **2015**, *13* (2015), 169−175.
(40) Davies, R. P. W.; Aggeli, A.; Beevers, A. J.; Boden, N.; Carrick, L. M.; Fishwick, C. W. G.; Mcleish, T. C. B.; Nyrkova, I.; Semenov. A. N., Self-assembling β-sheet tape forming peptides. *Supramol. Chem.* **2006**, *18* (5), 435–443.
(41) Mertens, H. D.; Svergun, D. I. Structural characterization of proteins and complexes using small-angle X-ray solution scattering. *J. Struct. Biol.* **2010**, *172* (1) 128–141.
(42) Wychowaniec, J. K.; Illiut, M.; Zhou M., Moffat J., Elsawy M., Pinheiro W., Hoyland J., Miller A., Vijayaraghavan A., Saiani A. Designing peptide/graphene hybrid hydrogels through fine-tuning of molecular interactions. Biomacromolecules **2018,** *19* (7), 2731–2741.
(43) Guilbaud, J.-B.; Saiani, A., Using small angle scattering (SAS) to structurally characterise peptide and protein self-assembled materials. *Chem. Soc. Rev.* **2011**, *40* (3), 1200–1210.
(44) Harkins, W. D.; Davies, E. C. H.; Clark, G. L., The orientation of molecules in the surfaces of liquids, the energy relations at surfaces, solubility, adsorption, emulsification, molecular association and the effect of acids and bases on interfacial tension. (Surface energy VI). *J. Am. Chem. Soc.* **1917**, *39* (4), 541–596.
(45) Harkins, W. D.; Keith, E. B., The oriented wedge theory of emulsions and the inversion of emulsions. *Science* **1924**, *59* (1534), 463–467.

(46) Mimica-Dukic, N.; Bozin, B.; Sokovic, M.; Simin, N., Antimicrobial and antioxidant activities of Melissa officinalis L. (Lamiaceae) essential oil. *J. Agric. Food Chem.* **2004**, *52* (9), 2485–2489.
(47) Serra, E.; Hidalgo-Bastida, L. A.; Verran, J.; Williams, D.; Malic, S., Antifungal Activity of Commercial Essential Oils and Biocides against Candida Albicans. *Pathogens* **2018,** *7* (1), 1–12.
(48) Schnitzler, P.; Schuhmacher, A.; Astani, A.; Reichling, J., Melissa officinalis oil affects infectivity of enveloped herpesviruses. *Phytomedicine* **2008,** *15* (9), 734–740.
(49) Angelini, P.; Tirillini, B.; Akhtar, M. S.; Dimitriu, L.; Bricchi, E.; Bertuzzi, G.; Venanzoni, R., Essential Oil with Anticancer Activity: An Overview. In Anticancer Plants: Natural Products and Biotechnological Implements: Volume 2, Akhtar, M. S.; Swamy, M. K., Eds. Springer Singapore: Singapore, **2018**, 207–231.

For Table of Contents Use Only

Aromatic stacking facilitated self-assembly of ultra-short ionic complementary peptide sequence: β-sheet nanofibres with remarkable gelation and interfacial properties

Jacek K. Wychowaniec,[a,b,c] Ronak Patel,[d] James Leach,[d] Rachel Mathomes,[d] Vikesh Chhabria,[d] Yogita Patil-Sen,[d] Araida Hidalgo-Bastida,[e,f,g] Robert T. Forbes,[d] Joseph M. Hayes,[d] Mohamed A. Elsawy*[a,b,d,h]

[a] School of Materials, University of Manchester, Oxford Road, Manchester M13 9PL, UK
[b] Manchester Institute of Biotechnology, Oxford Road, Manchester M13 9PL, UK
[c] School of Chemistry, University College Dublin, Belfield, Dublin 4, Ireland
[d] School of Pharmacy and Biomedical Sciences, University of Central Lancashire, Preston PR1 2HE, UK
[e] Centre for Biosciences, Department of Life Science, Manchester Metropolitan University, Manchester, M1 5GD, UK
[f] Centre for Musculoskeletal Science and Sports Medicine, Manchester Metropolitan University, Manchester, M1 5GD, UK
[g] Centre for Advance Materials and Surface Engineering, Manchester Metropolitan University, Manchester, M1 5GD, UK
[h] Leicester Institute of Pharmaceutical Innovation, Leicester School of Pharmacy, De Monfort University, The Gateway, Leicester LE1 9BH, UK

* Corresponding author: Phone: +44(0)1163664581; e-mail: mohamed.elsawy@dmu.ac.uk

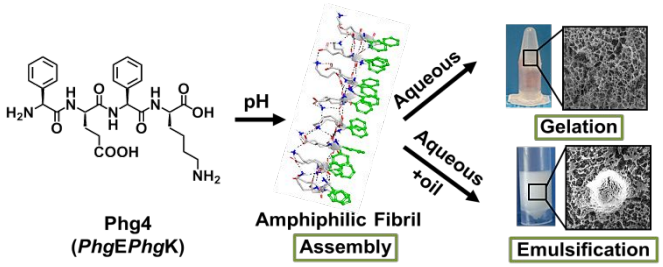

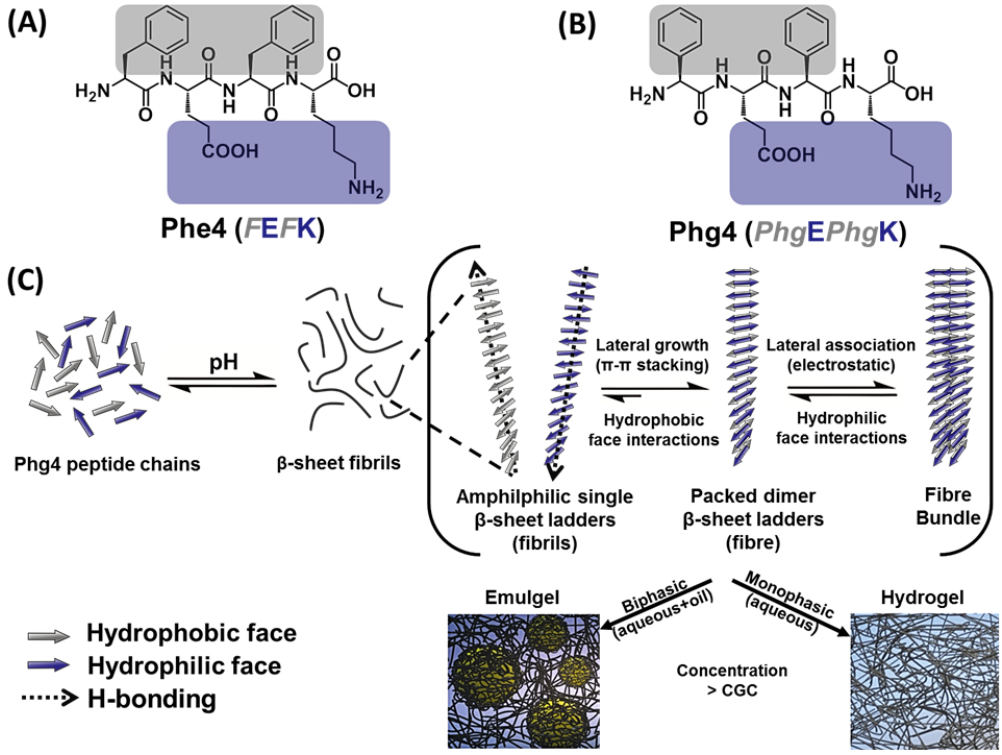

Figure 1: Molecular structures of A) Phe4 (*FEF*K) and B) Phg4 (*Phg*E*Phg*K) peptides. (*F* – phenylalanine, E – glutamic acid, K – lysine, *Phg* – phenylglycine). C) Schematic illustration of Phg4 self-assembly into the amphiphilic β-sheet single ladder form, though π-stacking of the aromatic rings alongside the intermolecular H-bonding between backbone amides. The single ladder form is in equilibrium with the more thermodynamically stable packed β-sheet ladders in aqueous medium, where the latter is formed by lateral growth through hydrophobic interactions of the aromatic rings projecting from the hydrophobic face. In monophasic medium, the packed form is more abundant forming nanofibres, which above critical gelation concentration (CGC) entangle into a nanofibous network forming hydrogels. In oil-water biphasic media, the amphiphilic single ladder will adsorb on the oil-water interface forming oil-in-water (O/W) emulgel. The hydrophobic face is denoted by grey colour and the hydrophilic by violet.

254x190mm (96 x 96 DPI)

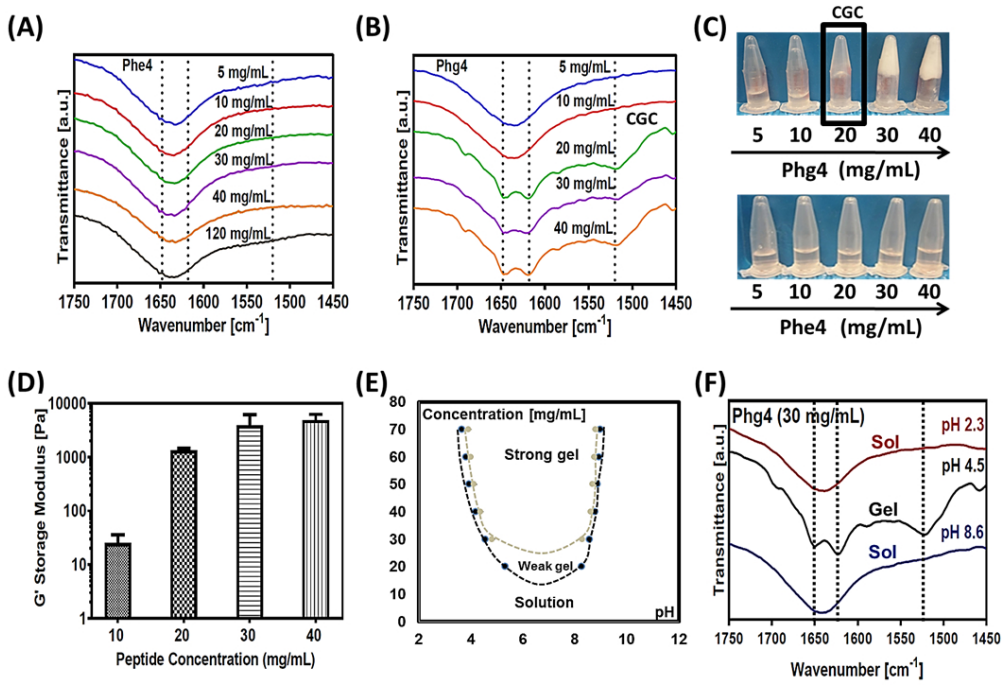

Figure 2: ATR-FTIR spectra for the two peptides: A) Phe4 and B) Phg4 at a series of concentrations. C) Inverted vial test of Phg4 (top panel) and Phe4 (bottom panel) peptides at pH 5. D) Shear modulus (G') (y axis set to log10) of Phg4 hydrogels at 6 rad s-1 obtained from the frequency sweep experiments performed at 0.2% strain. E) Phase diagram of Phg4 peptide as a function of pH and concentration. Three distinctive states were observed: strong gel, weak gel, and solution. F) ATR-FTIR spectra for Phg4 (30 mg/mL) showing phase transition from unstructured sol form at pH 2.3 to β-sheet gel form at pH 4.5 and back to unstructured sol form at pH 8.6.

279x190mm (96 x 96 DPI)

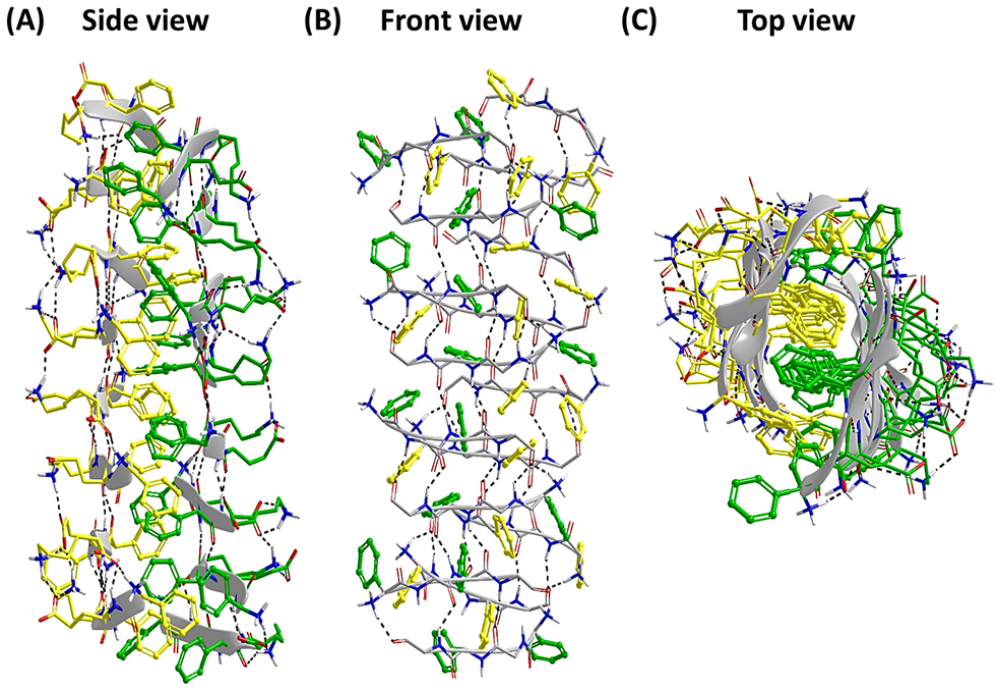

Figure 3: Predicted most stable packed dimer aggregation model from the PM7 calculations: A) side-view, B) front-view, with K and E sidechains omitted to more clearly demonstrate the inter-chain backbone hydrogen bonding and the phenyl ring stacking interactions and C) top-view. The RMSDs between the PM7 model and the model from the initial Prime side-chain predictions were 1.5 A^{o} and 2.2 A^{o} for backbone and sidechain, respectively, suggesting a good quality initial model from Prime but with PM7 theoretically more robust in terms of π-stacking optimization.[39]

259x179mm (96 x 96 DPI)

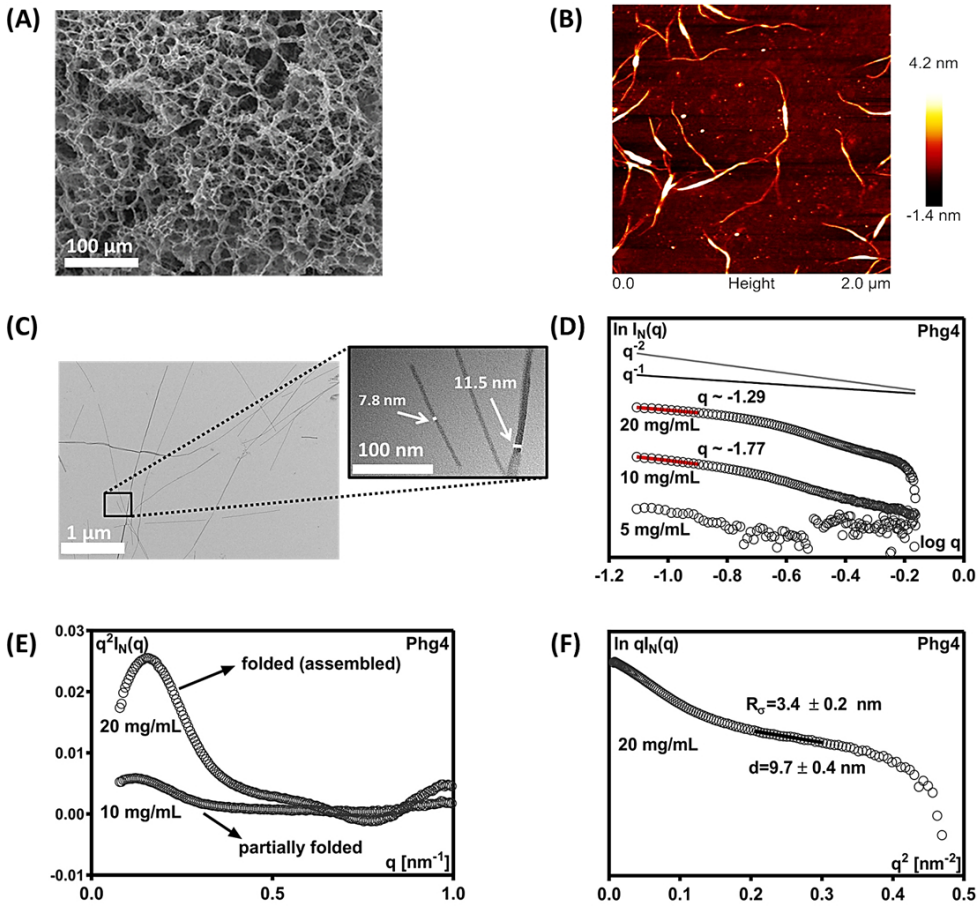

Figure 4: A) SEM image of 10X diluted and freeze-dried Phg4 hydrogel at 30 mg/mL. B) AFM micrographs of Phg4 hydrogel at 30 mg/mL diluted to 0.5 mg/mL. C) TEM micrographs of 10X diluted Phg4 hydrogel at 40 mg/mL, with arrows pointing to fibre bundles of ~7-11 nm size. D) ln[IN(q)] vs log q representation of SAXS of 5, 10 and 20 mg/mL of Phg4. q^{-1} *and* q^{-2} behaviour are also presented. E) Kratky plot (q^2 *IN(q)* versus *q* representation) of 10 and 20 mg/mL Phg4. The curve shapes are marked by arrows corresponding to folded (assembled) and partially folded states. F) SAXS scattering pattern of a 20 mg/mL Phg4 at low *q* plotted in a *ln[qIN(q)]* versus q^2 representation.

300x279mm (96 x 96 DPI)

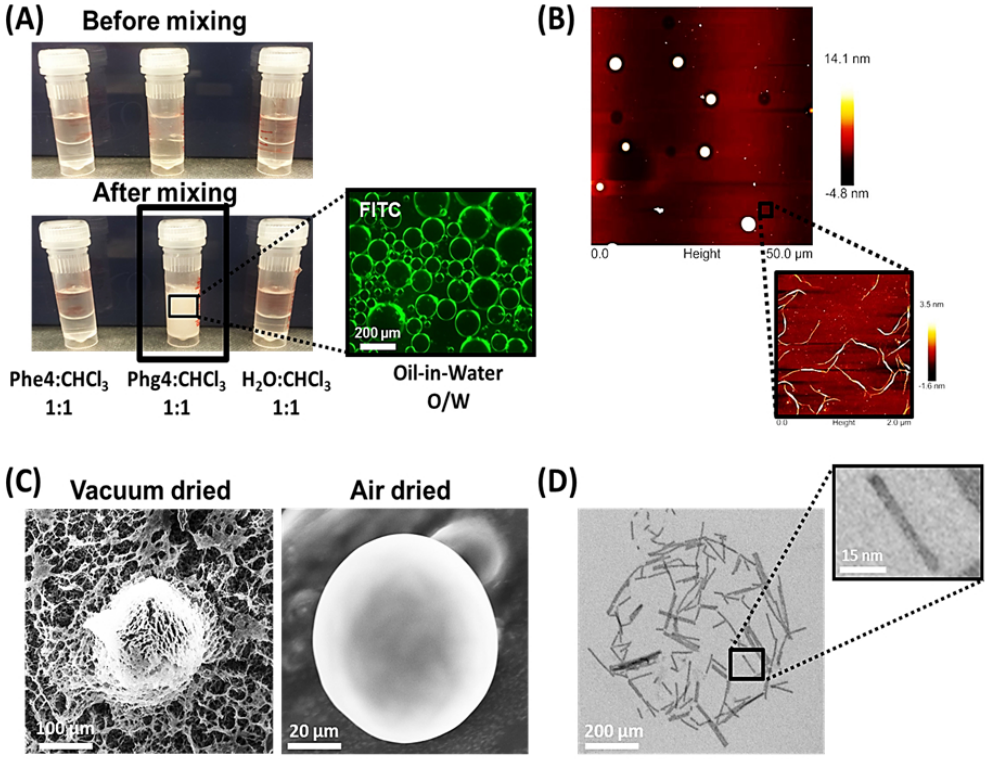

Figure 5: A) Photograph of 20 mg/mL Phe4 and Phg4 water chloroform ($CHCl_3$) mixtures at 1:1 volume ratio before and after mixing. Fluorescence microscopy image confirmed the formation of Phg4 oil-in-water (O/W) emulsion with the continuous aqueous phase stained with Fluorescein Isothiocyanate (FITC). B) AFM of Phg4-$CHCl_3$ emulsion showing microspheres formed at the oil-water interface at 1:1 volume ratio after sample drying. Background region close to the sphere shows individual fibrils similar to those observed in hydrogels (Figure 3B). C) SEM micrographs of a 30 mg/mL emulgel prepared at 1:1 W:O ratio, which has been 10X diluted and either vacuum dried (left) or air dried (right). D) TEM micrographs of 10X diluted Phg4 chloroform-in-water at 30 mg/mL, showing short fibre bundles of ~9 nm size arranged in a sphere like shape.

243x190mm (96 x 96 DPI)

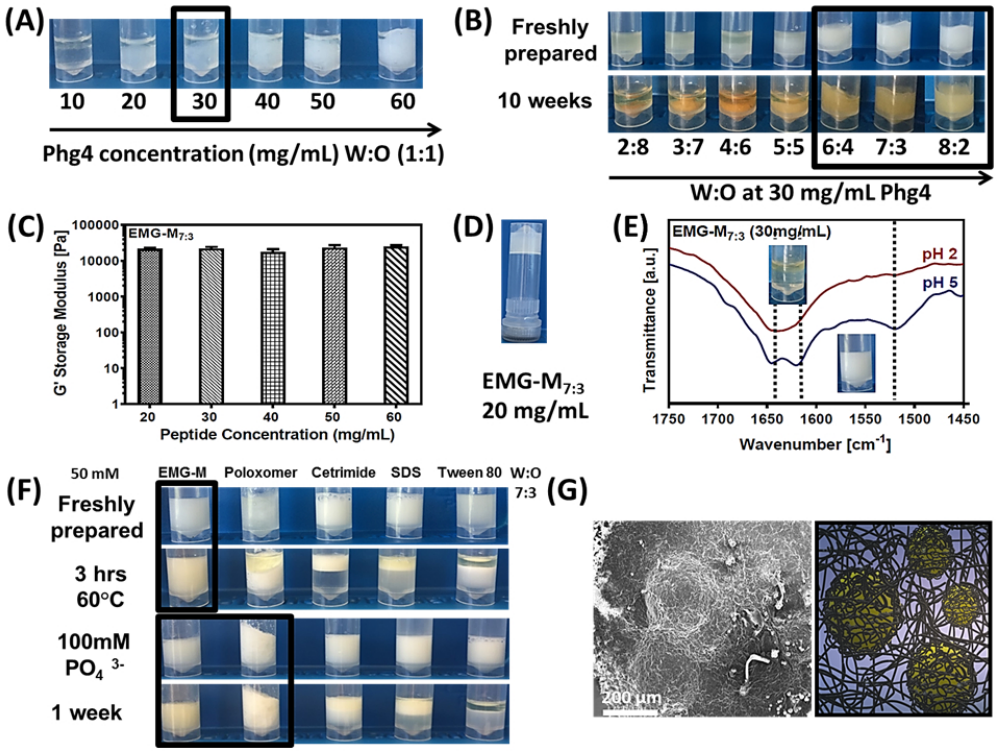

Figure 6: A) A series of Phg4 Melissa oil mixtures with a range of peptide concentrations (10-60 mg/mL) at 1:1 W:O volume ratio. B) EMG-M (30 mg/mL) mixed at a range of different W:O volume ratios (2:8-8:2) tested for phase separation over 10 weeks at room temperature. C) Shear moduli (G') of EMG-$M_{7:3}$ at a range of peptide concentrations (20-60 mg/mL), performed at 6 rad s^{-1} obtained from the frequency sweep experiments performed at 0.2% strain D) Inverted vial test of EMG-$M_{7:3}$ (20 mg/mL) at pH 5. E) ATR-FTIR spectra of EMG-$M_{7:3}$ (30 mg/mL) showing phase transition from unstructured immiscible form at pH 2to β-sheet structured emulgel form at pH 5 F) Emulsion stability profiles of EMG-$M_{7:3}$ versus poloxomer (Pluronic F-68), cetrimide (alkyltrimethylammonium bromide), sodium dodecyl sulphate (SDS) and tween 80 at 50mM emulsifier concentration after incubation for 3hrs at 60°C (top panel) and after incubation with 100mM potassium phosphate monobasic for 1 week (bottom panel). G) Left: SEM image of EMG-$M_{7:3}$ (30 mg/mL), which has been 10X diluted and vacuum dried, showing two oil droplets stabilized by peptide fibrous network at the interface. Right: illustration of the O/W EMG-M showing the Melissa oil droplets in yellow entrapped within the peptide nanofibrous network suspended in the continuous aqueous hydrogel phase in blue.

254x190mm (96 x 96 DPI)

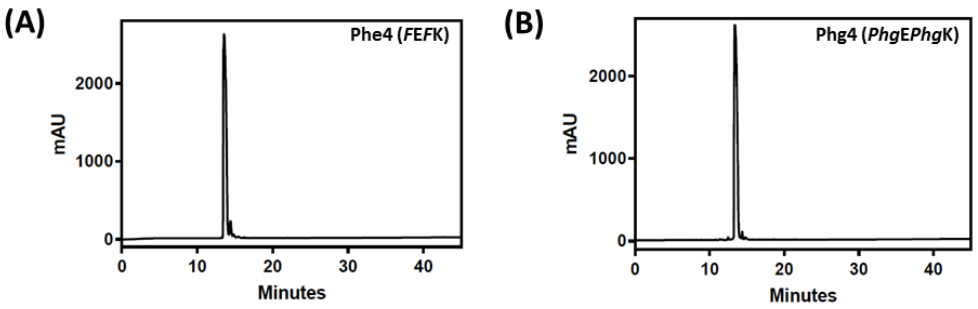

Figure S1: RP-HPLC chromatograms of A) Phe4 (F*E*F*K) and B) Phg4 (*Phg*E*Phg*K) peptides used. Peptide solutions (1 mg/mL in 1% trifluoroacetic acid in water/acetonitrile 50/50 V/V) injected on Phenomenex Jupiter column (4µ Proteo column 90A°, 250x4.66mm) equipped with UV detector (λ220 nm). Elution gradient was used (flow rate of 1mL/min, started from 90% solvent A (0.05% TFA in H2O)/10% solvent B (0.05% TFA in CH3CN) to 30% solvent A/70% solvent B in 45 minutes). Peptides purity was estimated as >95% as calculated from area under the peak data.

243x80mm (96 x 96 DPI)

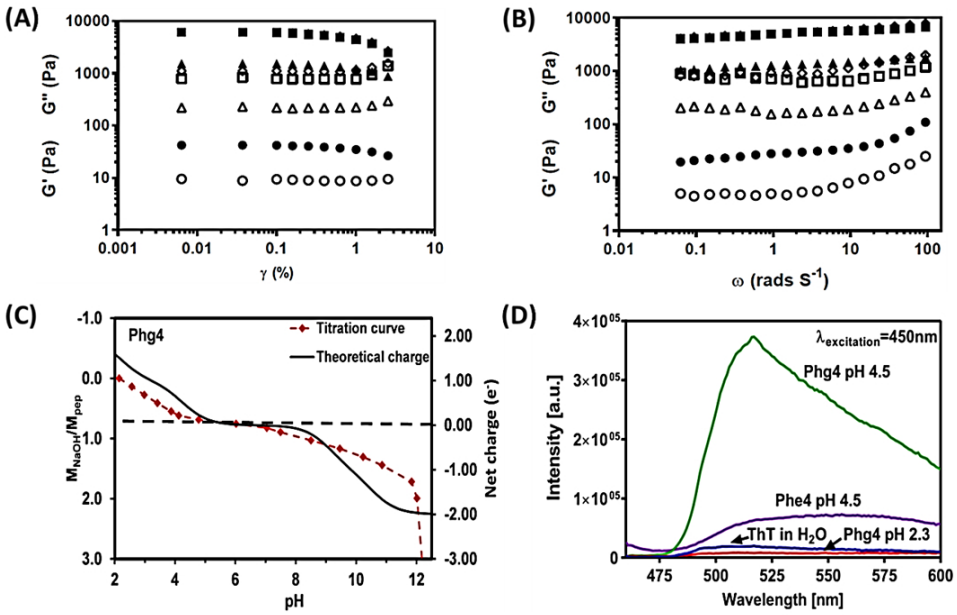

Figure S2: Figure S2: Oscillatory rheology characterisation for Phg4 hydrogels A) strain sweep at angular frequency (ω) 6 rad s^{-1} and B) Frequency sweep at strain (γ) 0.2%, within linear viscoelastic region, at peptide concentrations 10 mg/mL (●, ○), 20 mg/mL (▲, Δ),30 mg/mL (■, □) and 40 mg/mL (⧫, ◇) (close symbols: G′; open symbols: G″). C) Theoretical net charge state on Phg4 peptide (calculated from equation S1 here below) as a function of pH and molar ratio of added NaOH solution to the Phg4 peptide solution (M_{NaOH}/M_{pep}) as a function of pH. The experimental titration curve indicates that the net peptide charge is neutral (dashed line indicating zero net charge) within the self-assembly and gelation pH range (pH 4.5-8) when compared to the theoretical charge curve. D) ThT fluorescence showing significant enhancement of intensity for Phg4 at pH 4.5 compared to pH 2.3 indicating the formation of β-sheet fibres, which was marginal for Phe4 at pH 4.5 Z=Σ_i▒N_i 〖10〗^(〖pKa〗_i)/(〖10〗^pH+〖10〗^(〖pKa〗_i))-Σ_j▒N_j 〖10〗^pH/(〖10〗^pH+〖10〗^(〖pKa〗_j)) (S1) where Ni/j are the numbers and pKai/j the pKa values of the basic (i - pKa > 7) and acidic (j - pKa < 7) groups present on the peptide.[6]

293x190mm (96 x 96 DPI)

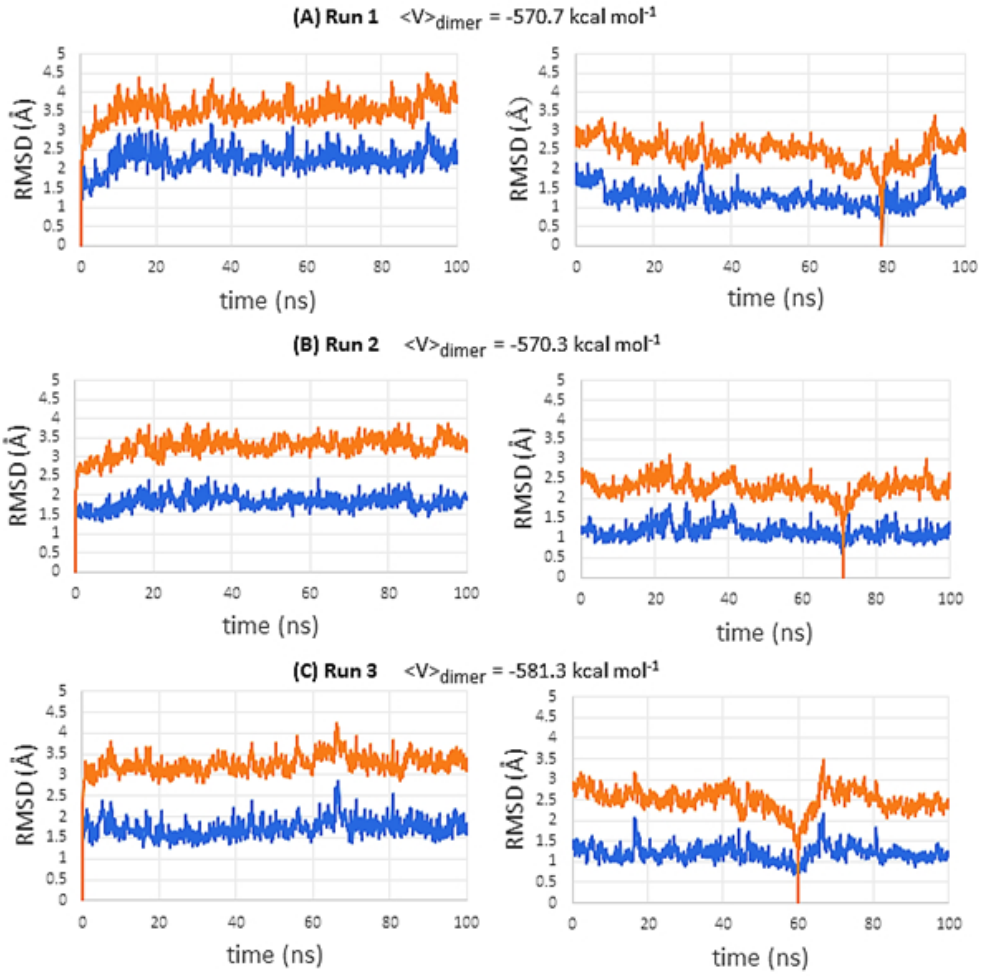

Figure S3: RMSDs backbone (blue) and sidechain (orange) of the aggregated packed Phg4 dimer model over the course of the three independent 100 ns MD simulations. On the left, the frame at time 0 ns was used as reference, while on the right, the reference frame was the representative from the largest trajectory cluster. The RMSD between the reference configuration and itself is zero by definition. Backbone RMSDs for the right-hand plots are small (close to ~1 A^{o}) and can be associated with thermal fluctuations. The average packed dimer potential energies $<V>_{dimer}$ are also reported, calculated using Prime and frames from the last 80 ns of each simulation, as described in the Molecular Dynamics Details.

159x159mm (96 x 96 DPI)

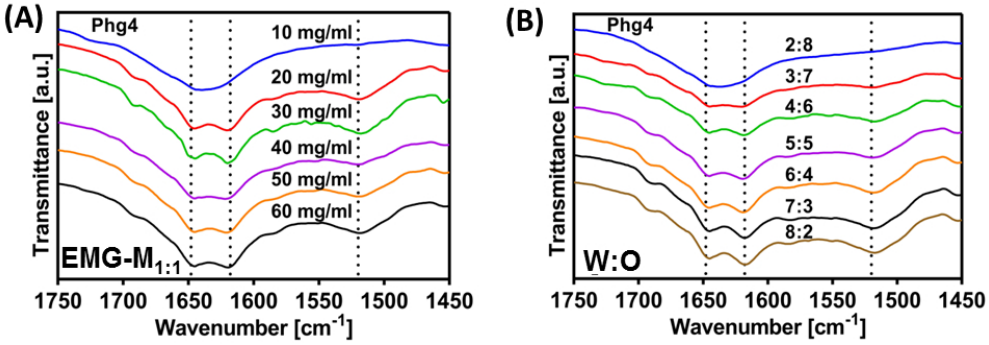

Figure S4: A) ATR-FTIR spectra for the of Phg4 Melissa oil mixtures at a series of peptide concentrations (10-60 mg/mL) at 1:1 W:O volume ratio (EMG-$M_{1:1}$), corresponding to the emulgel formation test (Figure 5A). B) ATR-FTIR spectra for EMG-M (30 mg/mL) mixed at a range of different W:O volume ratios (2:8-8:2) corresponding to the emulgel formation test (Figure 5B).

254x91mm (96 x 96 DPI)

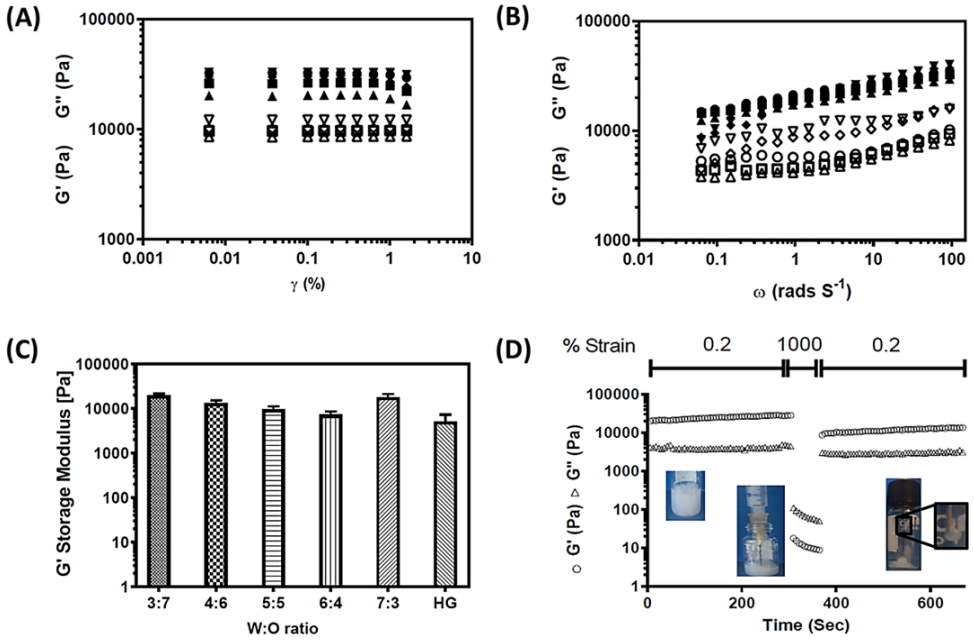

Figure S5: Oscillatory rheology characterisation for EMG-$M_{7:3}$ emulgels A) strain sweep at angular frequency (ω) 6 rad s^{-1} and B) Frequency sweep at strain (γ) 0.2%, within linear viscoelastic region, at a range of peptide concentrations: 20 mg/mL (▲, Δ),30 mg/mL (■, □), 40 mg/mL (⧫, ◇), 50 mg/mL (●, ○) and 60 mg/mL (▼, ▽) (close symbols: G'; open symbols: G"). C) Shear moduli (G') of EMG-M at a range of different W:O volume ratios (2:8-8:2) compared to hydrogel (HG) at same peptide concentration (30 mg/mL) and pH (5) , performed at 6 rad s^{-1} obtained from the frequency sweep experiments performed at 0.2% strain D) Strain sweep profiles of EMG-$M_{7:3}$ (40 mg/mL) exposed to 0.2% strain for 5 minutes, followed by 1000% strain for 1 minute (simulating injection strain), followed by 0.2% strain for 5 minutes to allow for the gel recovery (O G', Δ G'').

293x190mm (96 x 96 DPI)

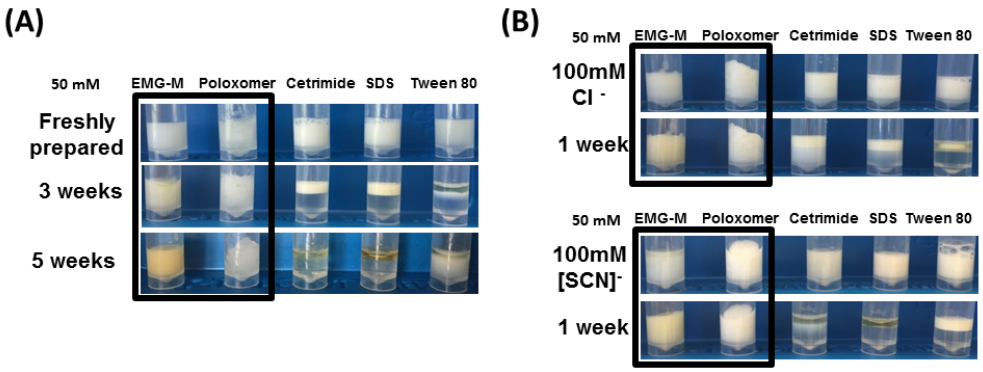

Figure S6: Emulsion stability profiles of EMG-$M_{7:3}$ versus poloxomer (Pluronic F-68), cetrimide (alkyltrimethylammonium bromide), sodium dodecyl sulphate (SDS) and tween 80 at 50mM emulsifier concentration A) storage at room temperature for 3-5 weeks, B) after incubation with 100mM sodium chloride (top panel) and potassium thiocyanate (bottom panel) for 1 week.

254x94mm (96 x 96 DPI)

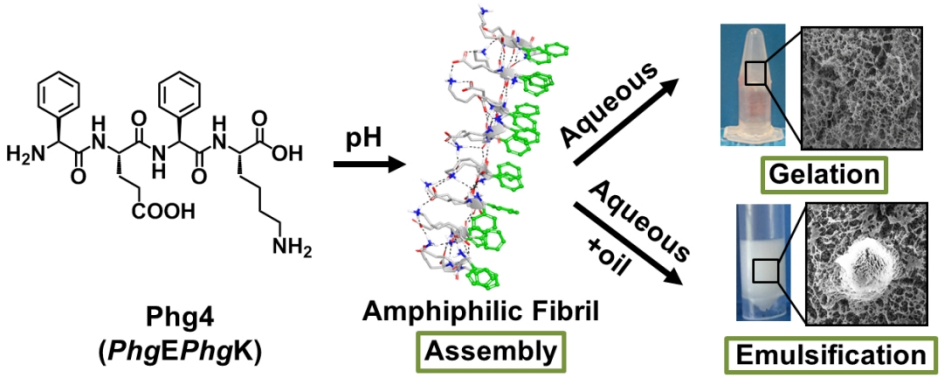

Graphical Abstract

350x139mm (96 x 96 DPI)